AD NUMBER
AD854585
LIMITATION CHANGES
TO: **Approved for public release; distribution is unlimited. Document partially illegible.**
FROM: **Distribution authorized to U.S. Gov't. agencies and their contractors; Administrative/Operational Use; FEB 1969. Other requests shall be referred to Air Force Rocket Propulsion Lab., Edwards AFB, CA.**
AUTHORITY
AFRPL ltr 29 Sep 1971

AFRPL-TR-69-39

TEST FIRING OF A CASTABLE CARBON ROCKET NOZZLE

J. R. ELLISON, LT, USAF
R. J. SCHONER
D. I. THRASHER

TECHNICAL REPORT AFRPL-TR-69-39

FEBRUARY 1969

AIR FORCE ROCKET PROPULSION LABORATORY
DIRECTORATE OF LABORATORIES
AIR FORCE SYSTEMS COMMAND
UNITED STATES AIR FORCE
EDWARDS, CALIFORNIA

AFRPL-TR-69-39

TEST FIRING OF A CASTABLE CARBON ROCKET NOZZLE

J. R. ELLISON, LT, USAF

R. J. SCHONER

D. I. THRASHER

FEBRUARY 1969

FOREWORD

This report was prepared by the Motor Component Development Branch, Solid Rocket Division, Air Force Rocket Propulsion Laboratory, (AFRPL). The subject test was conducted at the AFRPL under Project 305903AMG, Solid Rocket Hardware Design and Evaluation (SRHDE), with Lt John R. Ellison as Project Engineer. The nozzle being evaluated was procured from the Thiokol Chemical Corporation, Brigham, Utah, under Contract AF04(611)-11417 with Mr. Robert J. Schoner as Project Engineer for AFRPL. The Thiokol Chemical Corporation Project Engineer was Mr. Enos Bennion. The report describes a test conducted 30 October 1968. Mr. Durwood Thrasher performed the stress analysis portion of the accident investigation.

Samples of ablative blast pad covering materials were tested in a piggyback configuration for Philco-Ford, Aeroneutronic Division, Newport Beach, California. The Philco-Ford Project Engineer was Mr. Henry Blaes.

This report has been reviewed and approved.

CHARLES R. COOKE
Chief, Solid Rocket Division
Air Force Rocket Propulsion Laboratory

ABSTRACT

The test firing of a castable-carbon-material nozzle was conducted 30 October 1968 on the AFRPL 36-inch-diameter char motor, utilizing the Gilmore six-component thrust stand. Samples of blast pad covering material were also tested by insertion into the exhaust plume. The motor overpressured and performed erratically until approximately 19 seconds after ignition when the aft closure was ejected. Prior to the ejection, a burnthrough was observed at the aft closure - motor chamber interface. The incident resulted in severe damage to the motor and thrust stand, with minor damage to the test pad and adjacent facilities. Planned duration and chamber pressure had been 56 seconds and 750 psig respectively. The severe environment experienced by the nozzle allowed only limited acquisition of performance data. An accident investigation was initiated and the preliminary findings indicated that problems with the performance of uncured LPC 634-A propellant, characterized by massive side burning and possible burn-surface perturbations, caused the overpressurization. Improperly torqued closure attachment bolts allowed the burnthrough at the closure - motor interface. A description of stress analysis calculations performed for the bolted flange joint is provided.

BLANK PAGE

TABLE OF CONTENTS

APPENDIX - STRESS ANALYSIS CALCULATIONS

LIST OF TABLES

LIST OF ILLUSTRATIONS

LIST OF ILLUSTRATIONS

SECTION I

INTRODUCTION

This report describes the AFRPL 36-inch char motor test-firing of a castable carbonaceous material nozzle fabricated by the Thiokol Chemical Corporation. Also, blast pad covering materials were tested for Philco-Ford, Aeroneutronics Division, as an additional test item. The test resulted in overpressurization and destruction of the test motor approximately 18 seconds after ignition. Damage to the nozzle was limited to that inflicted by the severe high-chamber-pressure environment, even though the motor aft closure was ejected. Preliminary postfire data analysis and the initial results of a detailed accident investigation are included.

A. OBJECTIVE

This test was the sixth and final test conducted in support of Contract AF04(611)-11417 with the Thiokol Chemical Corporation. The program objectives were to develop and demonstrate a low-cost-castable or low-pressure-moldable carbonaceous material for use in ablative solid rocket nozzles. The first five nozzle tests demonstrated wide variations in material test results with tests 1 to 3 (Reference 1) exhibiting excellent performance and tests 4 and 5 showing very poor performance. The specific objective of this test was to reproduce the success of earlier tests by limiting the castable material usage to nozzle inlet and exit areas. Because test 5 had possibly failed due to poor throat insert performance, a proven regression-resistant material, G-90 graphite, was used in the throat to insure nozzle survivability.

The blast pad covering materials test was the fourth and last in a series of tests conducted at AFRPL to assist Philco-Ford in completing Contract F33615-67-C-1733. Extensive materials-performance data will be documented in the final report of that contract. Discussions of the

piggyback test will be limited to the contributions to the motor failure introduced by the method of installing the materials-testing fixture.

B. TEST HARDWARE DESCRIPTION

Hardware related to the castable carbon nozzle test could be divided into four general areas: the char motor, thrust stand, test nozzle, and materials-testing fixture. Each of these is described below.

Char Motor - The gas generator used for the test was the AFRPL 36-inch-inside-diameter char motor. The motor utilized silica filled buna-n rubber insulation that was reconditioned by cleaning between firings. The motor fired vertically upward using uncured propellant in an end-burner configuration.

Thrust Stand - The thrust stand used for the test was a six-component 20,000-pound thrust capacity unit manufactured by Gilmore Industries, Cleveland, Ohio. Figure 1 is an illustration of the char motor/thrust stand assembly during its initial calibration. A work platform surrounded the unit for the test firing. Normally, a six-component stand would not be used for a test such as the cast-carbon firing, but the stand had suffered damage during a previous test (Reference 2) and a checkout before the next TVC (Thrust Vector Control) system test firing was desirable.

Castable Carbonaceous Material Nozzle - Prefire photographs of the test nozzle are found in Figures 2, 3, and 4. Figure 5 illustrates the areas where castable carbon materials were utilized, and Table I outlines the formulation of the materials. Significant nozzle dimensions are listed in Table II.

Blast Pad Materials and Testing Fixture Materials tested are shown in Figure 6, and engineering sketches are shown in Figures 7, 8, and 9. A photograph of the assembly installed for the test is shown in Figure 10. The materials were not inserted into the exhaust plume as shown in

Figure 7, extended position, but were placed only as far as the outside edge of the plume. Limited actuator power necessitated this arrangement; the unit used did not supply enough force to evercome aerodynamic effects of the plume on the samples.

C. TEST PROGRAM

An uncured propellant, LPC 634-A, produced by the Lockheed Propulsion Company, was selected for the test. The propellant was a high-burn-rate, 5700° F-flame-temperature formation consisting of 17% aluminum, 68% ammonium perchlorate, 1.5% n-butyl ferrocene catalyst, and 14.5% PBAN binder/DOZ plasticizer mixture. The oxidizer consisted largely (27%) of fine, 7.9-micron-diameter particles. Desired test papameters were a 54-second duration at 750-psig chamber pressure. The blast pad materials were inserted in the plume 2 seconds after ignition and removed 2 seconds later.

D. TEST RESULTS

The char motor overpressured erratically, experienced a burnthrough at the aft closure-motor case interface, and ejected the aft closure. The six-component thrust stand was severely damaged, as was the char motor. Nozzle performance was poor in the areas of interest, the throat approach and exit cone. The effects of the overpressure probably influenced the poor performance, but the exact contribution could not be determined.

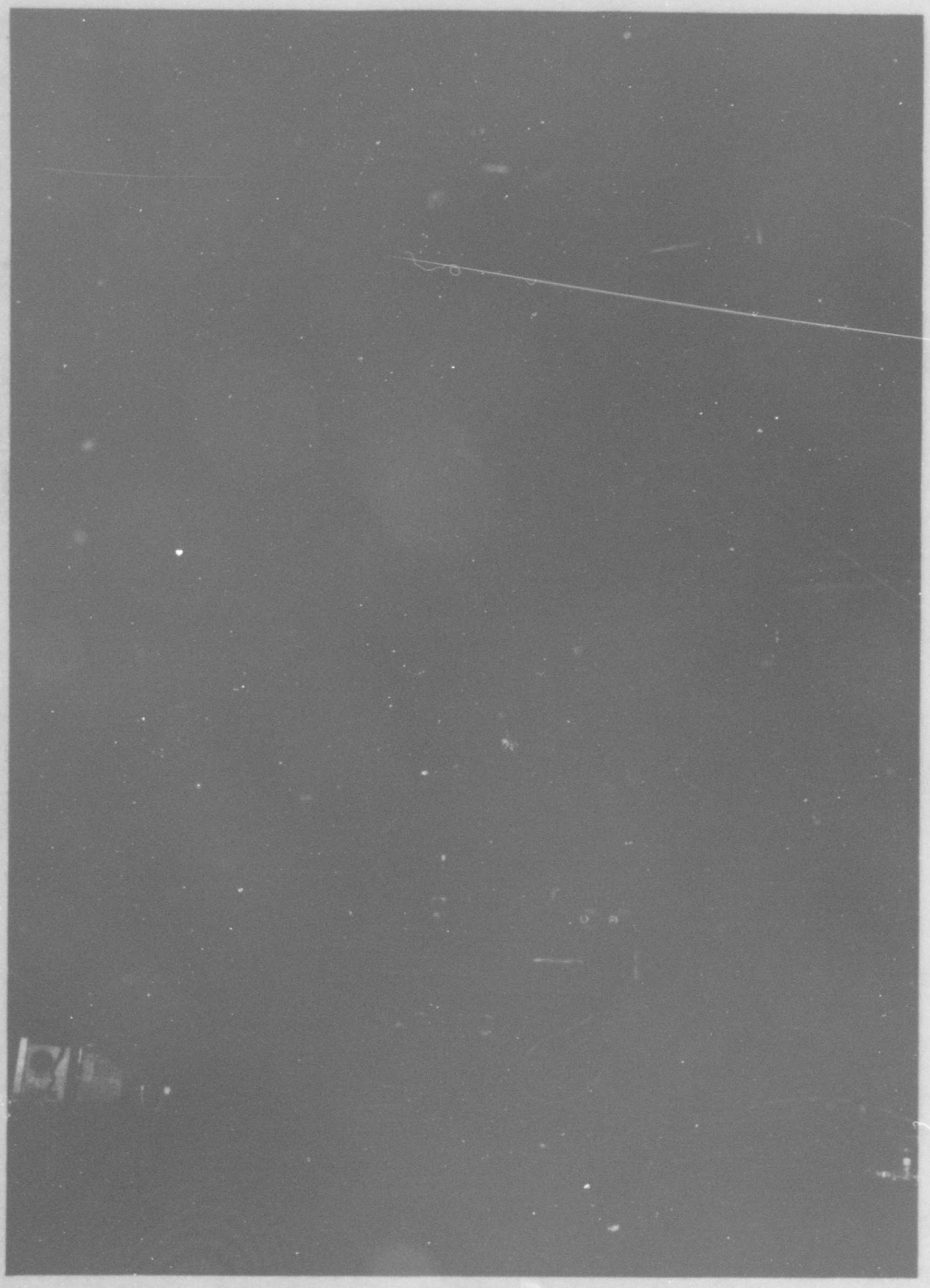

Figure 1. Char Motor and Thrust Stand Assembly

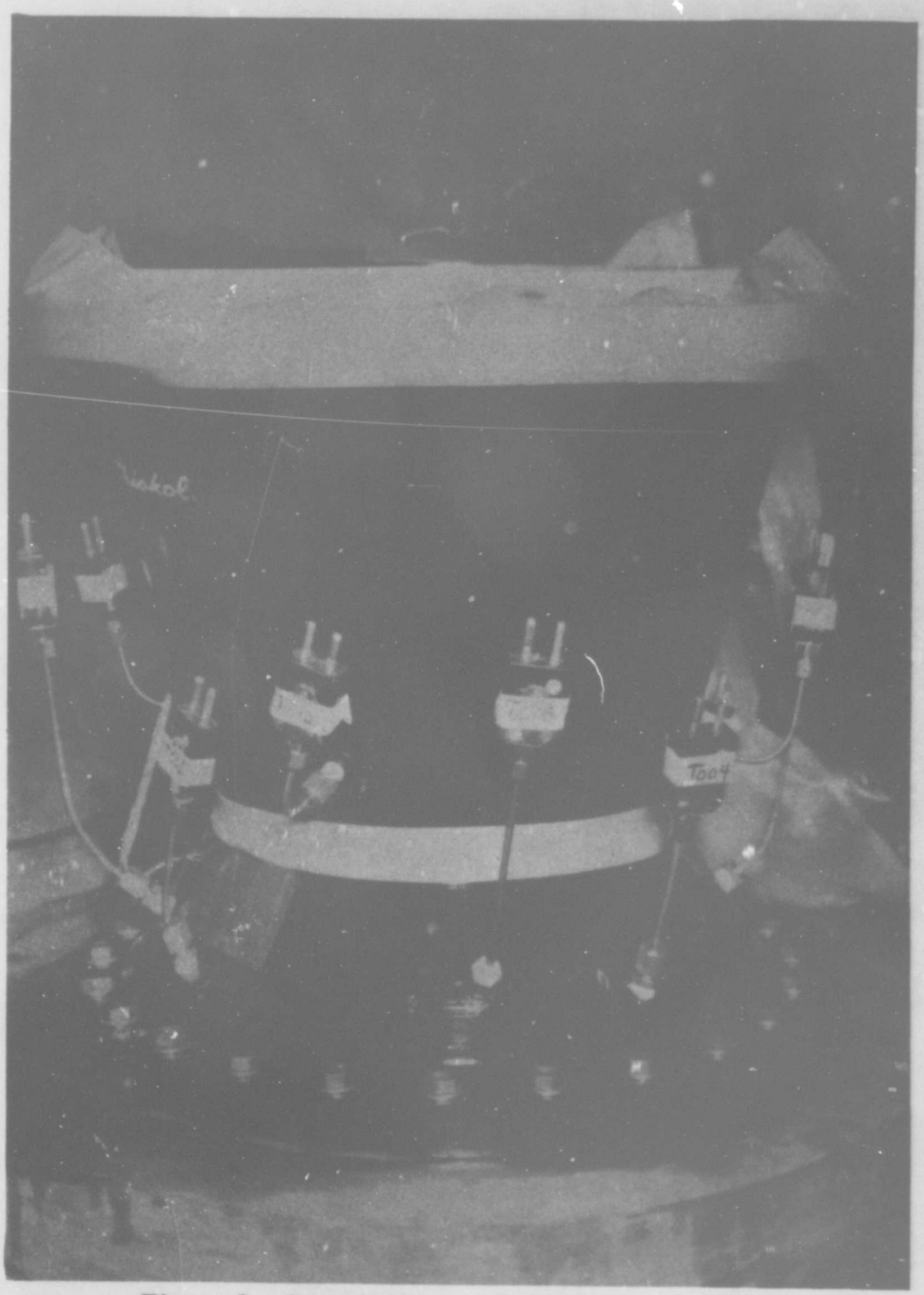

Figure 2. Overall View of Test Nozzle (Prefire)

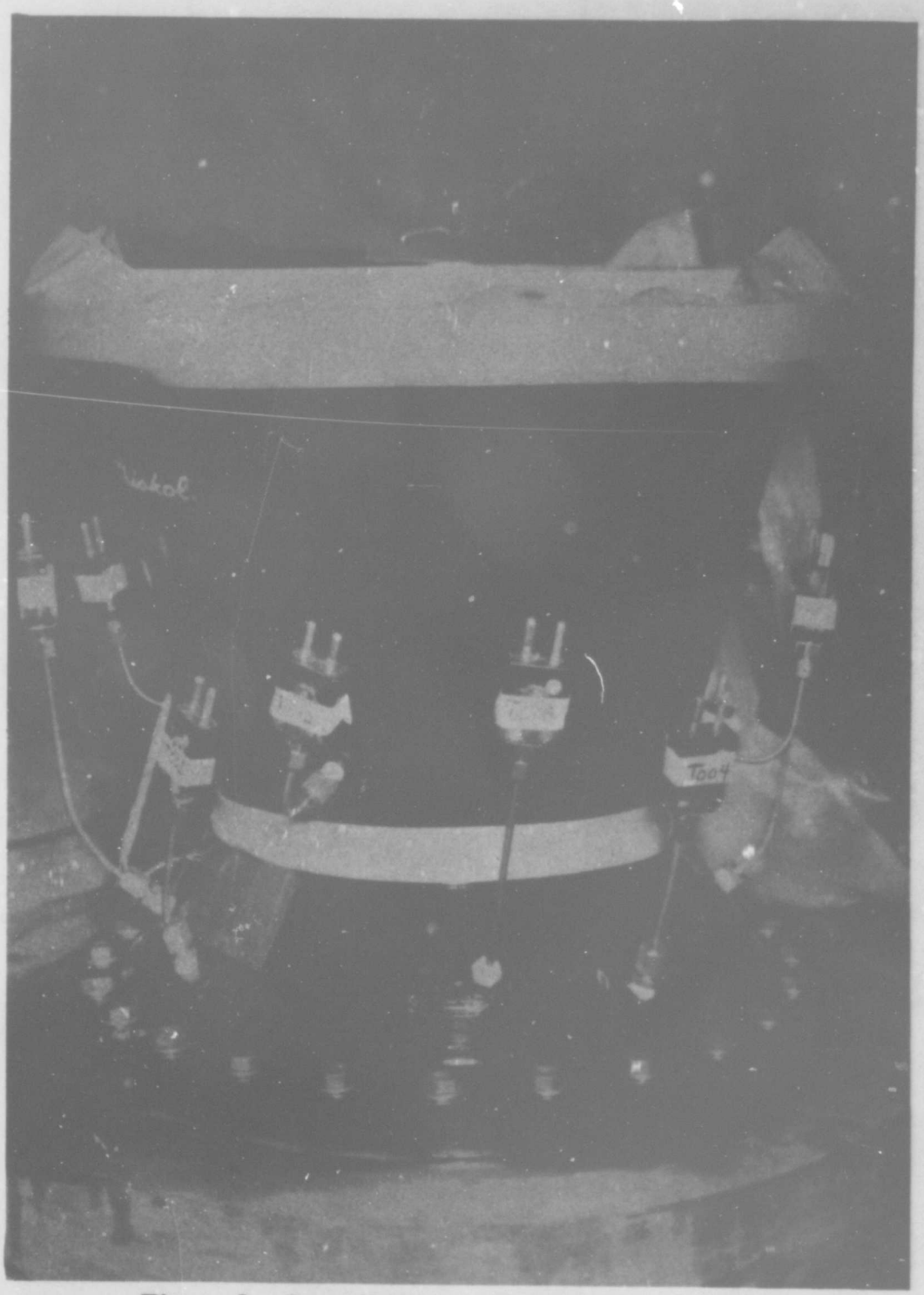

Figure 2. Overall View of Test Nozzle (Prefire)

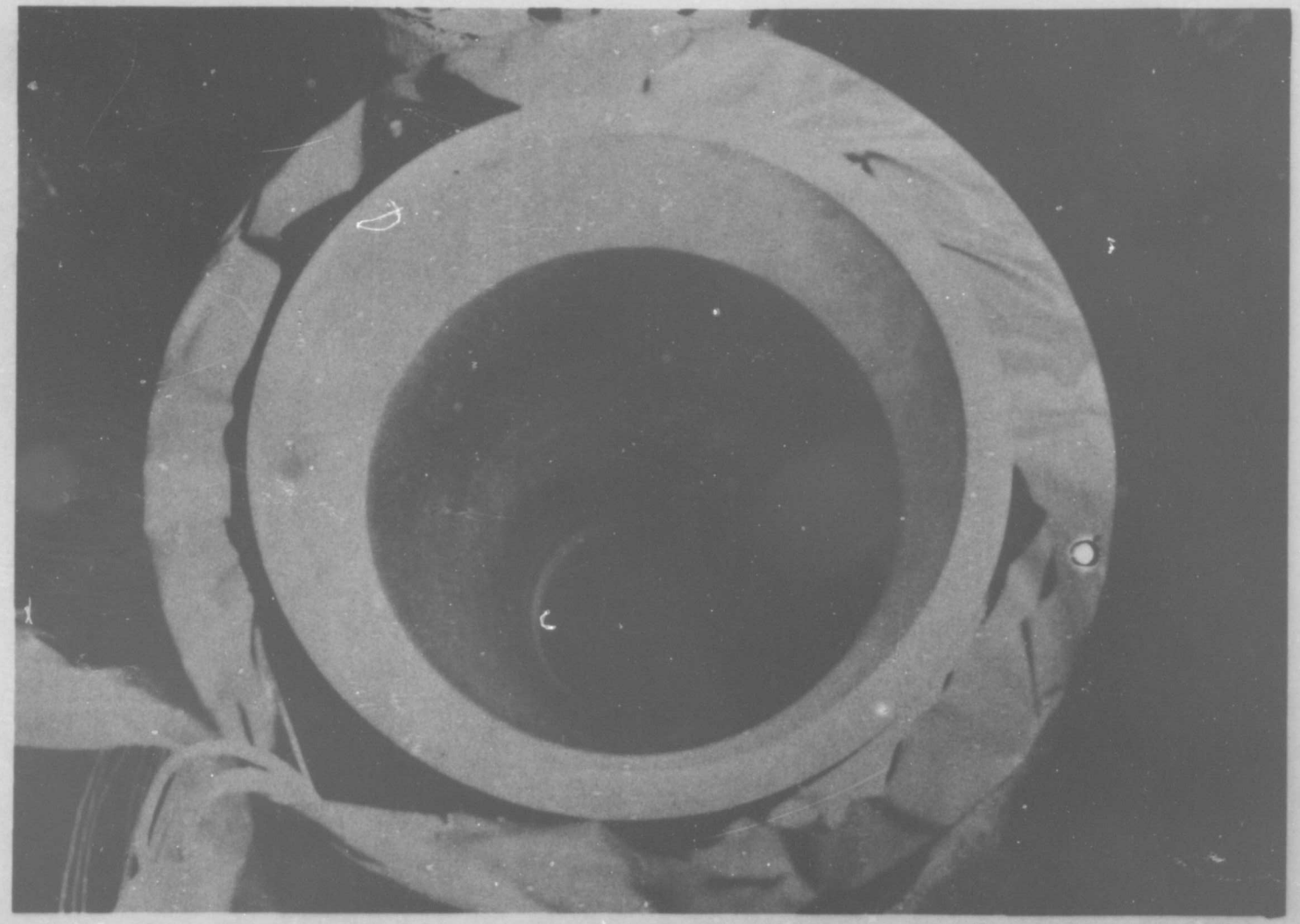

Figure 4. Castable Carbon Exit Cone Extension

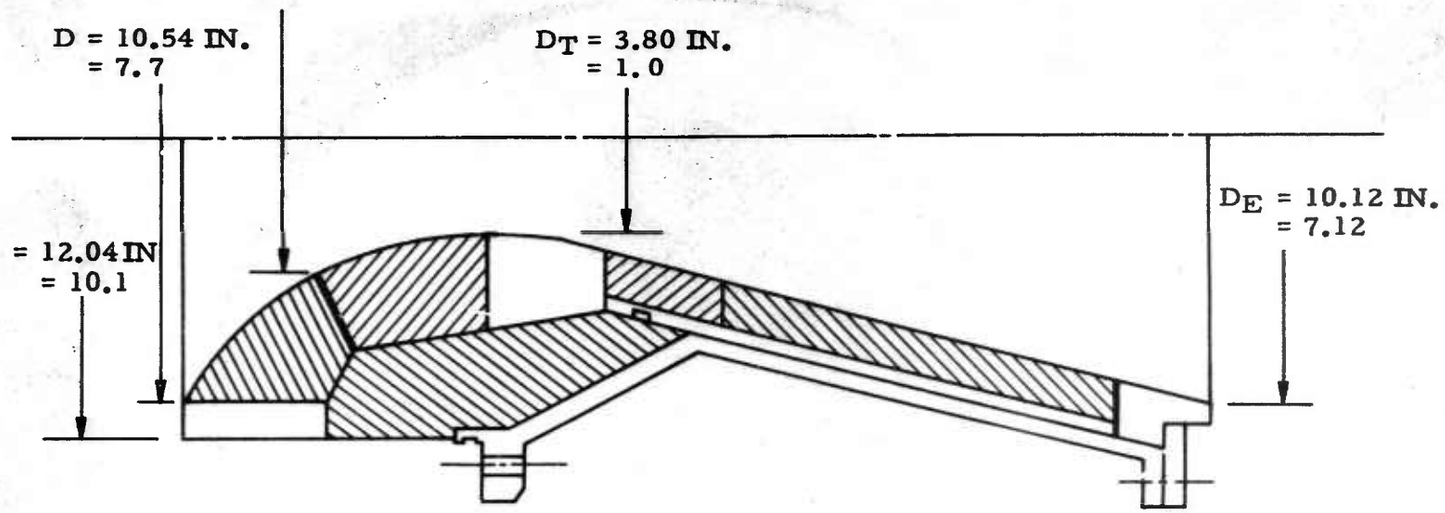

NOTE: SHADED AREA SIGNIFIES CAST CARBON MATERIALS

Figure 5. Nozzle Cross Section

TABLE I

NOZZLE MATERIALS AND FABRICATION PROCEDURES

MATERIAL	LOCATION	FABRICATION PROCESS	REMARKS
LCCM-2610	All entrance and exit cone liners	Mold at 1000 psi and 300° F, machine to final dimensions	Composed of 75% graphite particles and 25% Monsanto SC 1000 adhesive
G-90 graphite	Throat insert	Machine from commercial billet	-
1020 steel	Nozzle shell	Standard machining	-
LCMC-T-4113	Throat back-up	Trowel and cure at 200 psi and 300° F	-
Silica cloth phenolic	Exit come rerainer	Tape wrap parallel to centerline and cure at 200 psi, 300° F	-
Glass cloth phenolic	Exit cone insulator	Tape wrap parallel to centerline and cure at 200 psi, 300° F	-
Carbon cloth phenolic	Entrance cone overwrap	Tape wrap parallel to centerline	-

TABLE II

SIGNIFICANT MOTOR AND NOZZLE PERFORMANCE PARAMETERS

TEST TITLE TCC Castable Carbon TEST NUMBER 40-025	TEST DATE 30 October 1968
Propellant Formulation LPC - 634 A	
Theoretical Flame Temperature 5700° F	Ambient Temperature 68° F
Prefire Throat Diameter 3.80 in.	Ambient Pressure 13.8 psia
Postfire Throat Diameter 3.918	
Prefire Motor Diameter 37 7/8 in. nominal	Cast-to-Fire Time Interval 22 hours
As-Poured Propellant Depth 35 7/8 in.	
Prefire Propellant Depth 35 7/8 in.	
Prefire Propellant Temperature 65° F	
Propellant Weight 2550 lbs	Casting Method vacuum
Igniter(s) Used $BKNO_3$ BAG	
Strand Burn Rate $0.635\left(\frac{Pc}{800}\right)^{.3}$	
7-Inch Motor Burn Rate $0.70\left(\frac{Pc}{800}\right)^{.3}$	
Predicted Max Pc 700 psig	
Actual Max Pc 1440 psig	

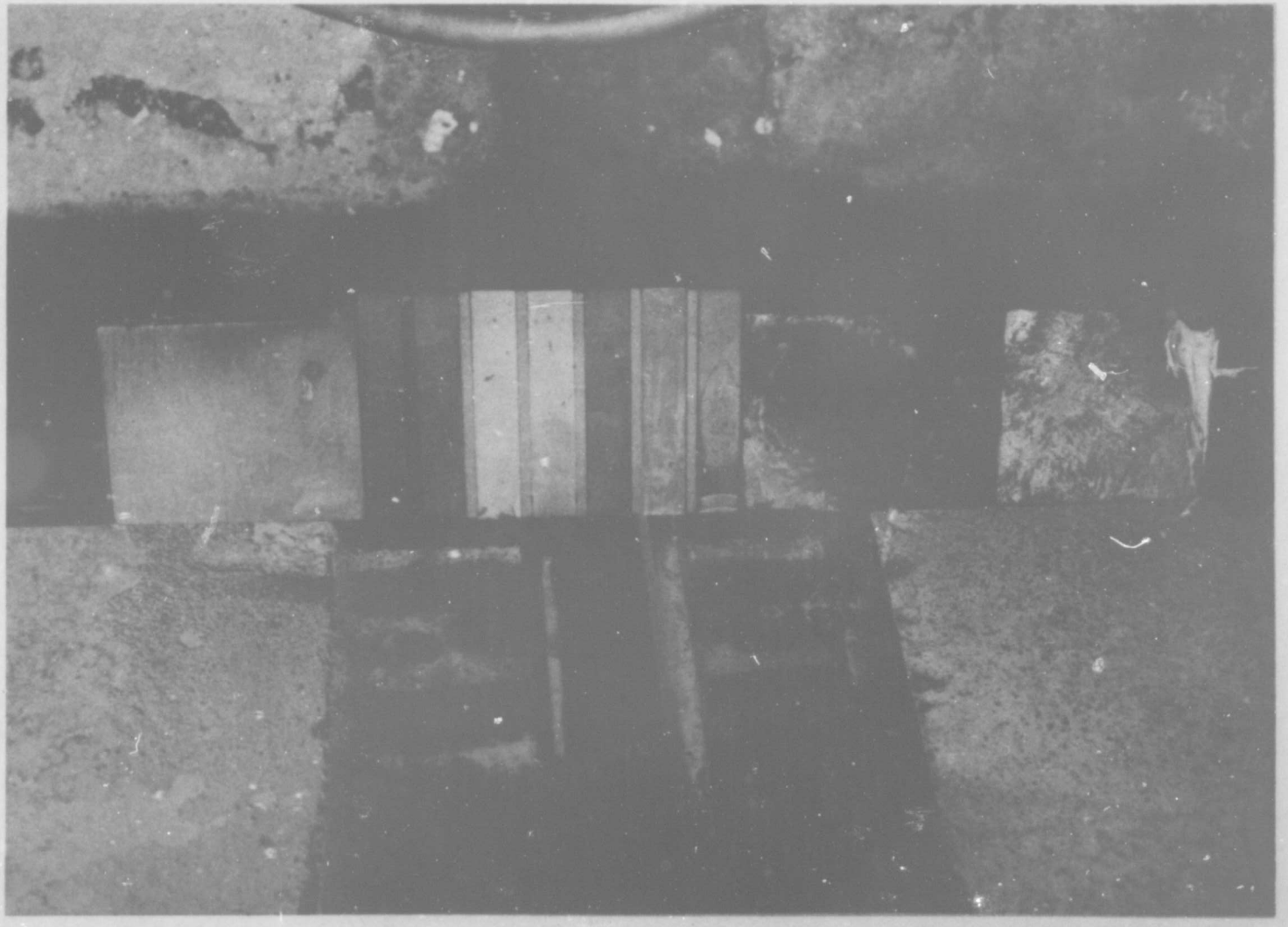

Figure 6. Blast Pad Materials

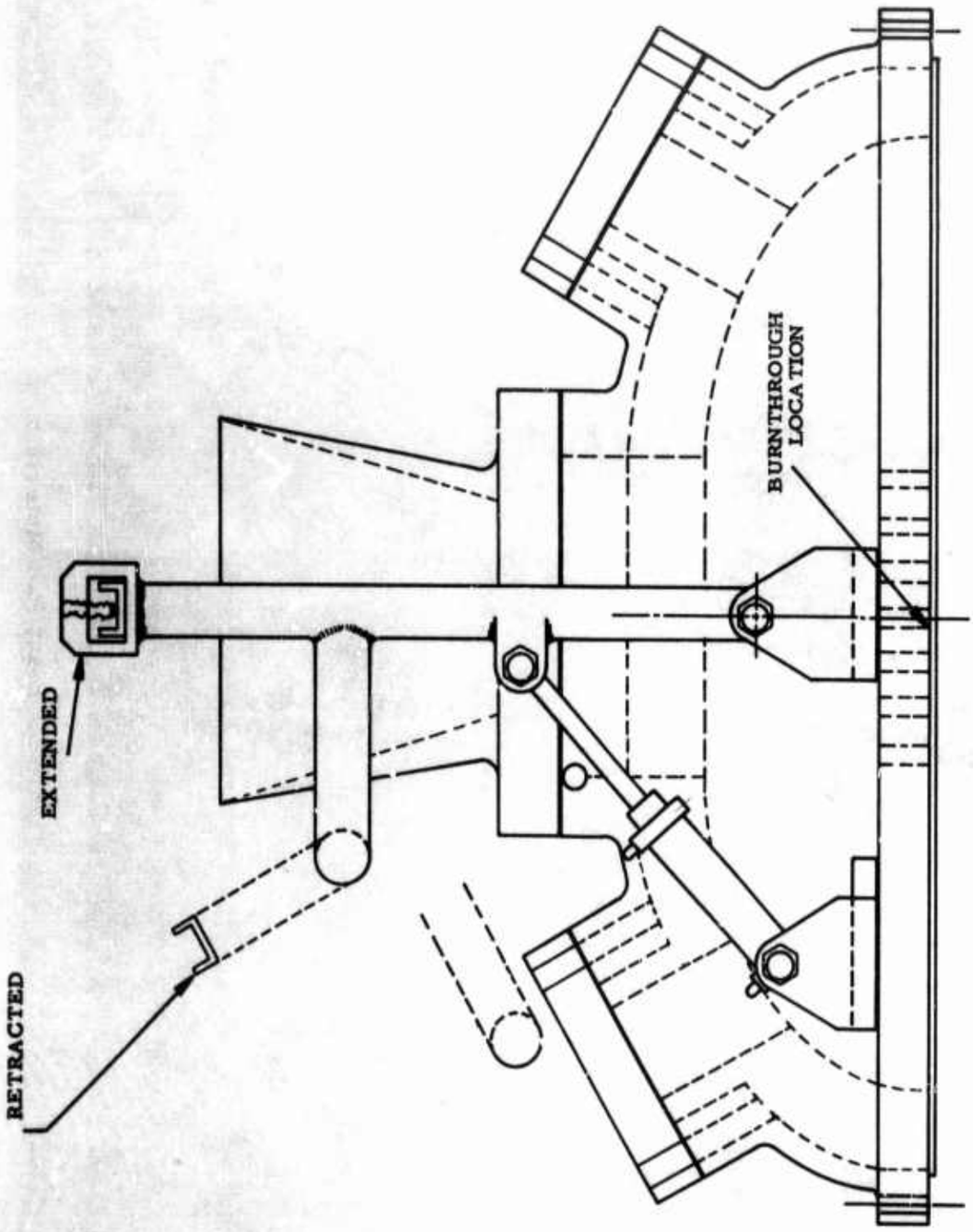

Figure 7. Materials Test Fixture, Side View

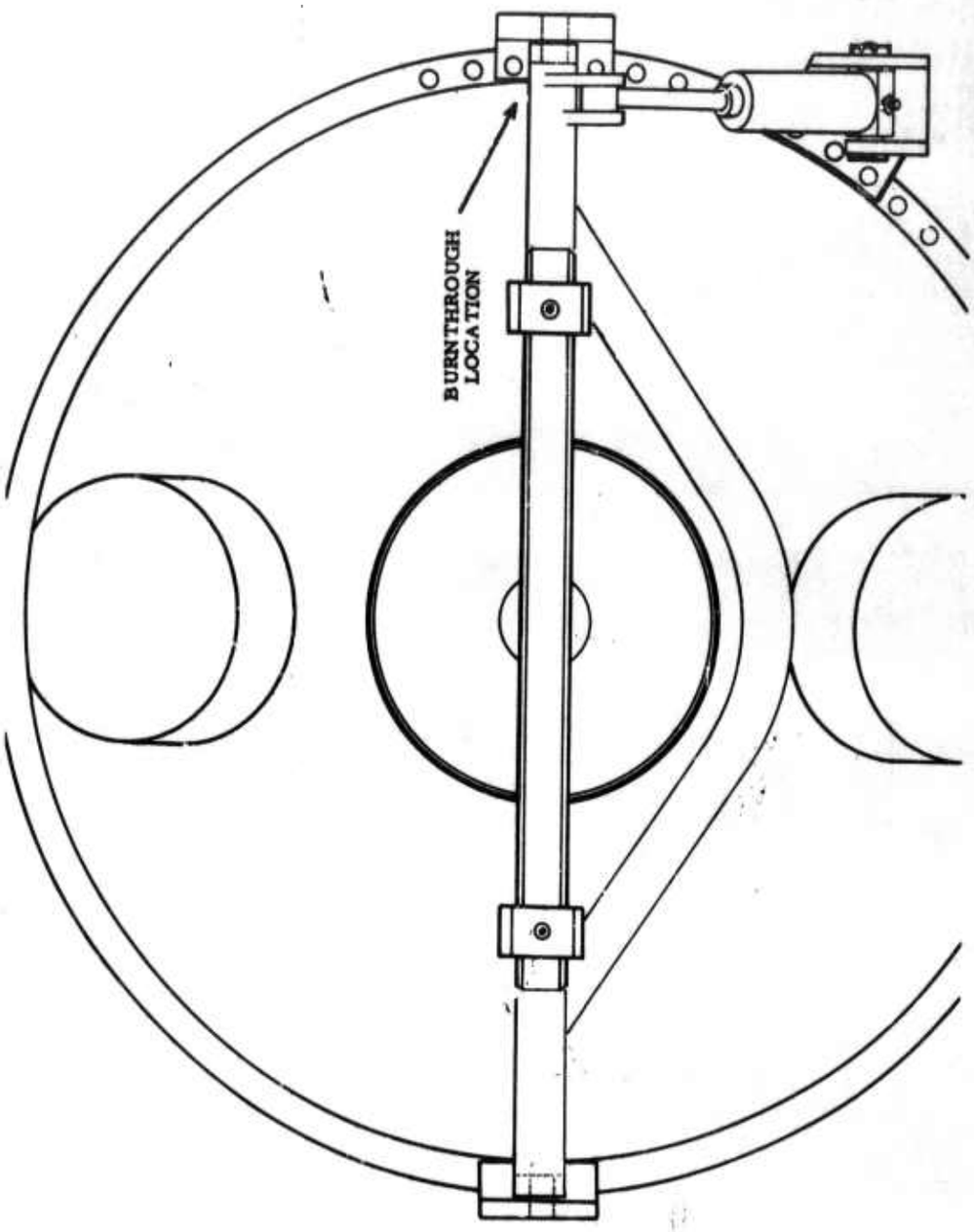

Figure 8. Materials Test Fixture, Top View

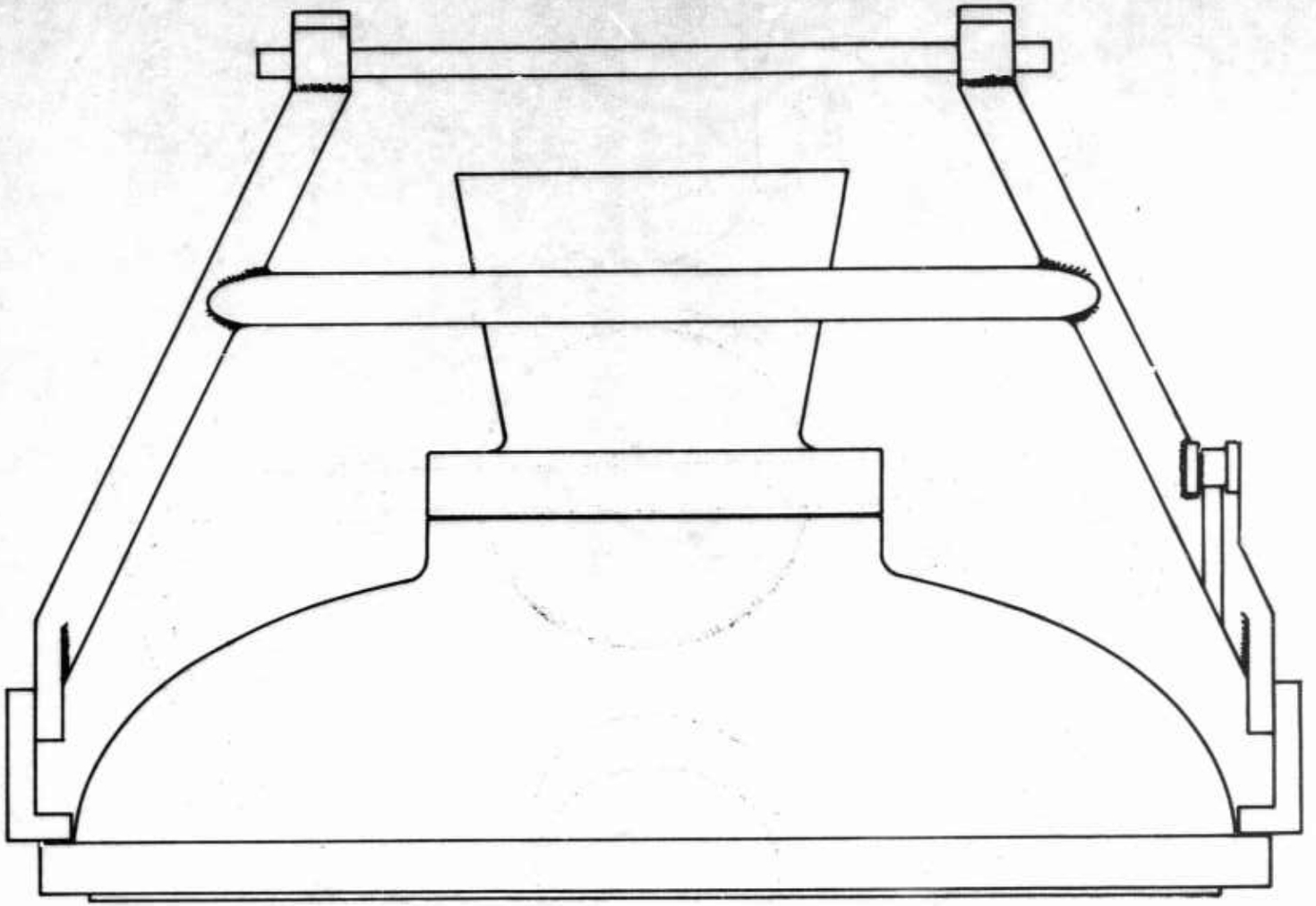

Figure 9. Materials Test Fixture, Rear View

Figure 10. Overall View of Fixture on Closure

SECTION II

MOTOR AND NOZZLE PERFORMANCE

The nozzle was received from Thiokol Chemical Corporation, and installed in the 36-inch char motor aft closure. Forty-eight hours prior to the scheduled motor loading, the chamber insulation was coated with PBAN polymer. Immediately before loading, the polymer was reapplied to insure an even coating. Vacuum casting fixtures were attached (Figures 11 and 12), and the propellant was loaded through a slit-plate deaerator. The aft closure was installed and the high-strength closure bolts torqued with a pneumatic wrench. The materials testing fixture was installed concurrent with the aft closure installation. Some difficulty was experienced during torquing of the bolts at the fixture attachment locations. This difficulty proved to be significant factor. A $BKNO_3$ bag igniter (see Figure 13) was installed 6 inches above the propellant surface and the motor was fired.

The chamber-pressure-versus-time trace is shown in Figure 14. Axial thrust versus time is shown in Figure 15. Indications of yaw and pitch versus time are shown in Figures 16 and 17, respectively. The values in these two figures are not correct side load measurements since they were not corrected for the geometry of the thrust stand. They are true indications of the relative magnitudes of forces, however, and do illustrate their time-dependent behavior.

A chronological listing of significant events is contained in Table III. There are variations between visual and digital times for the occurrence of all events, but none affect the overall sequence of events. To summarize the motor performance, the following narrative is provided:

Figure 11. Vacuum Casting Fixture

Figure 12. Vacuum Casting Fixture

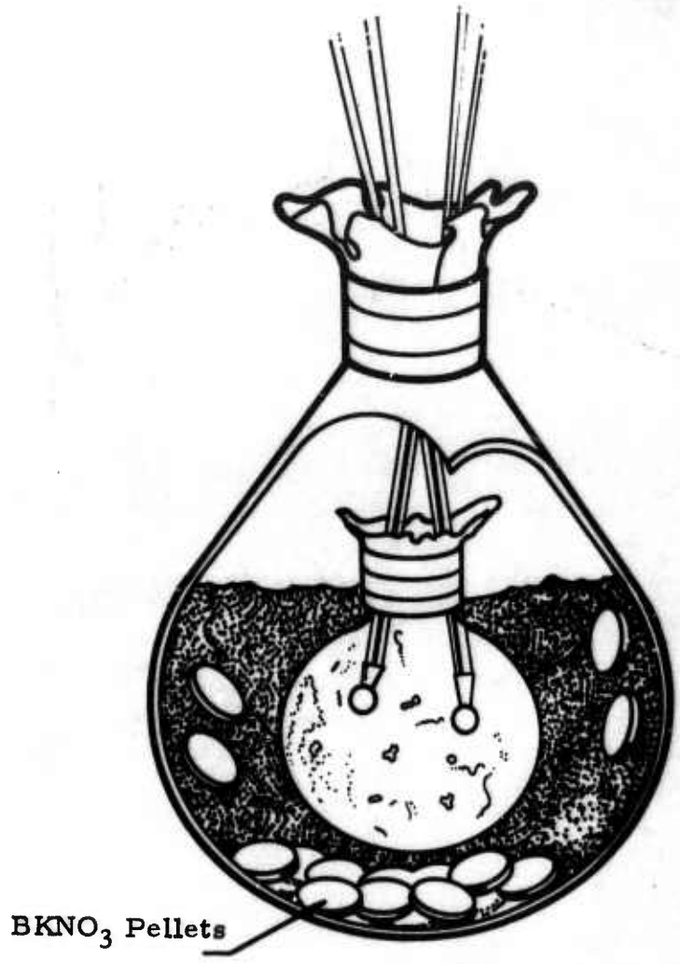

Figure 13. Bag Igniter (Typical)

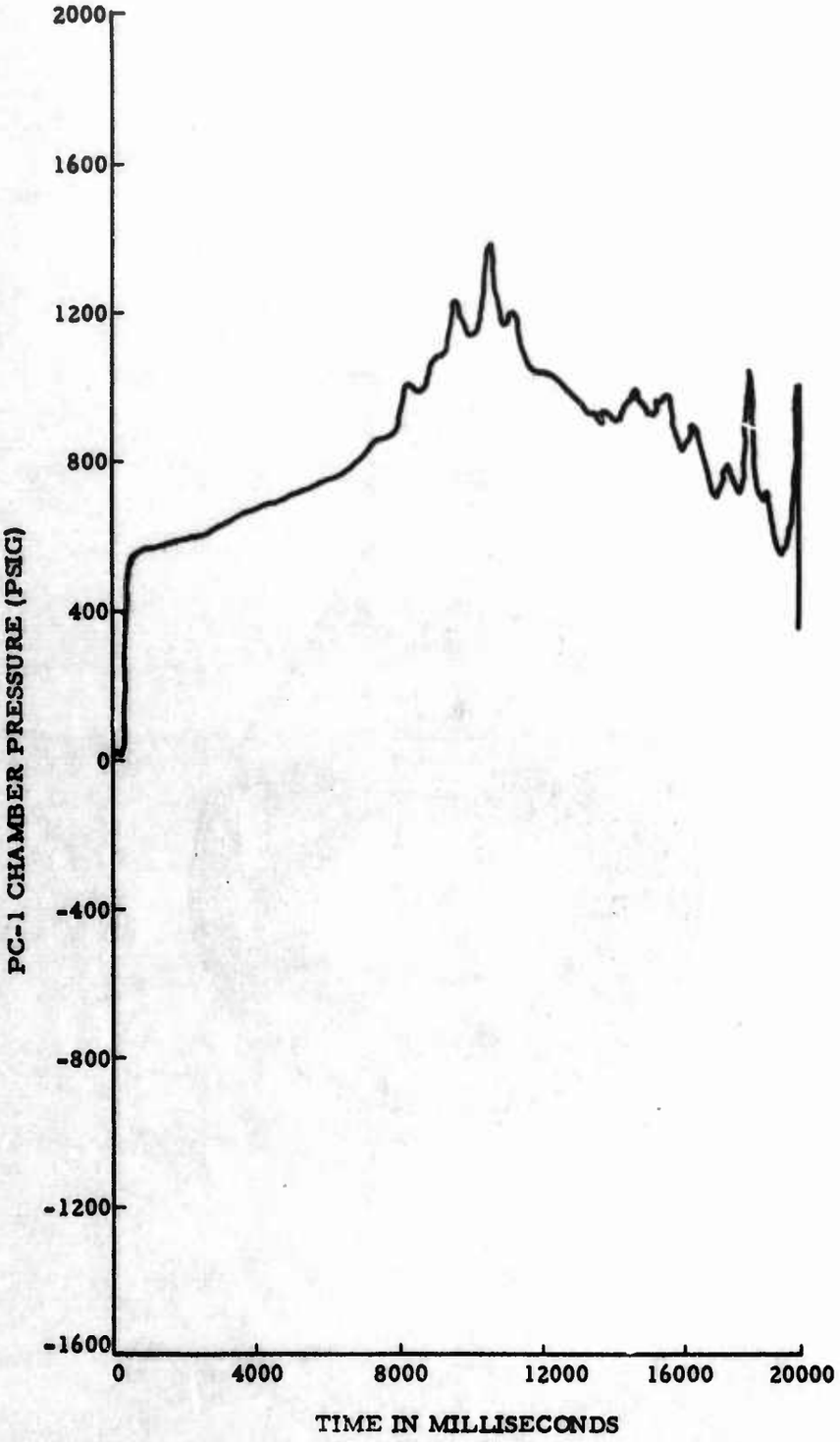

Figure 14. Chamber Pressure versus Time

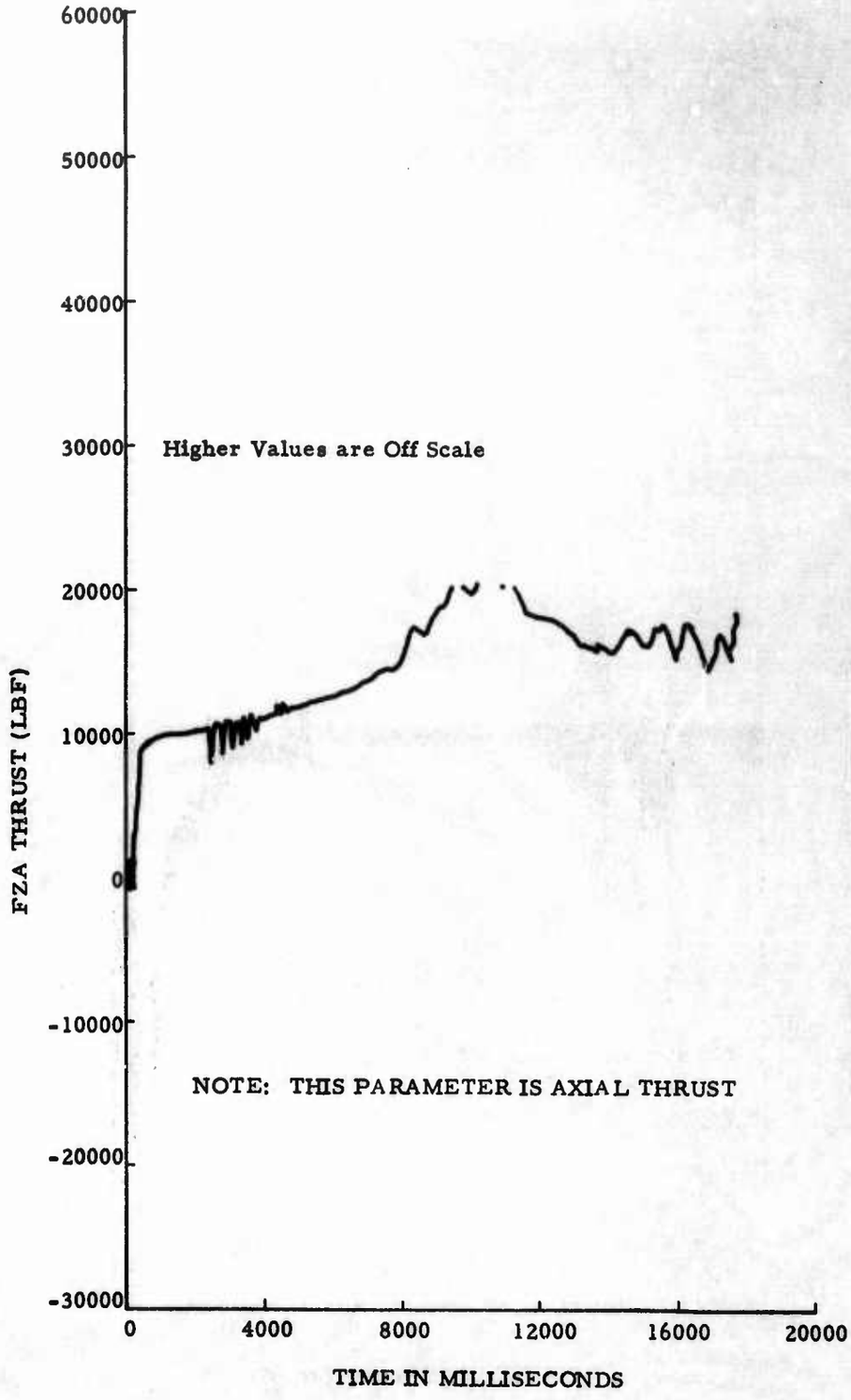

Figure 15. Axial Thrust versus Time

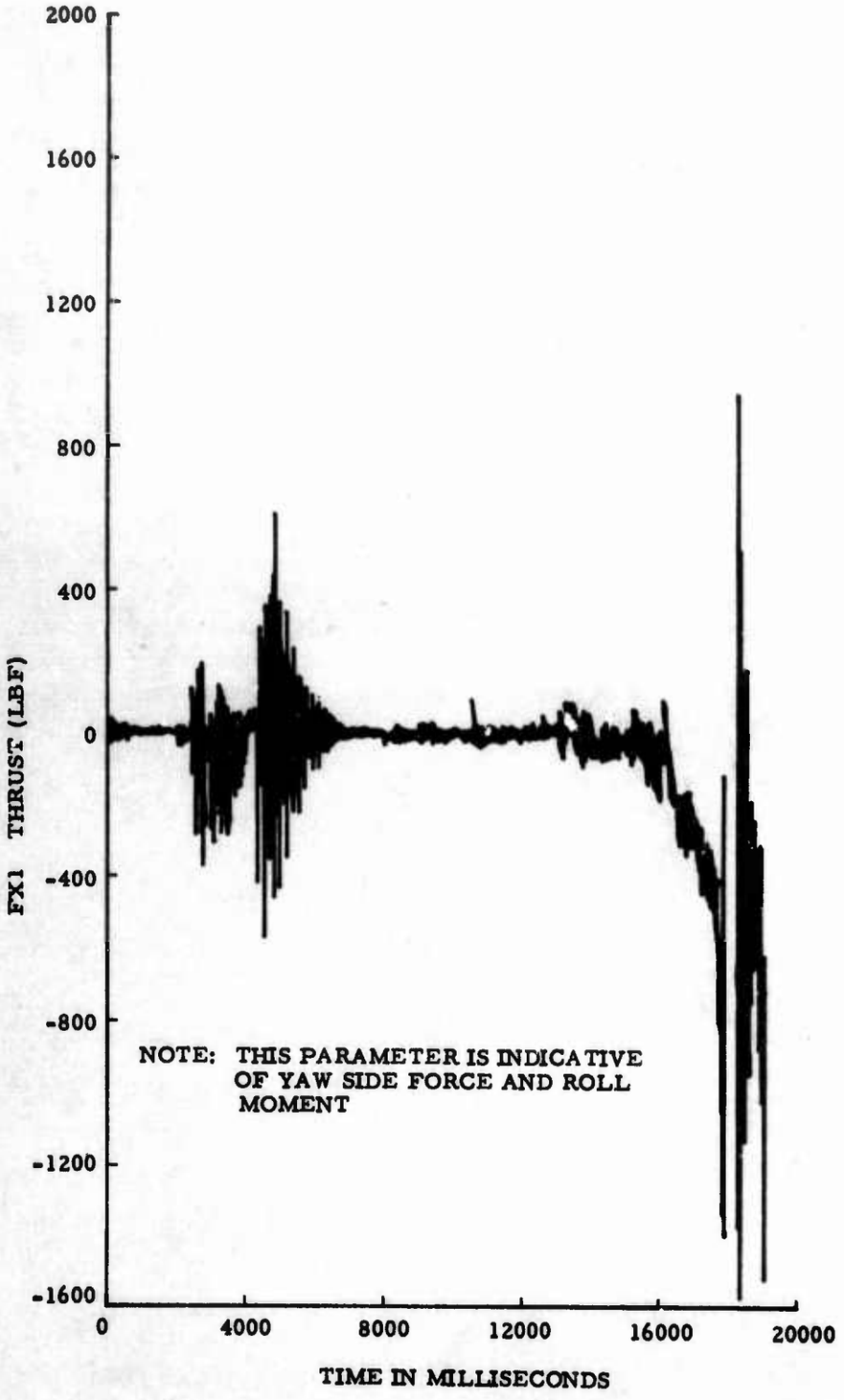

Figure 16. Yaw Force versus Time

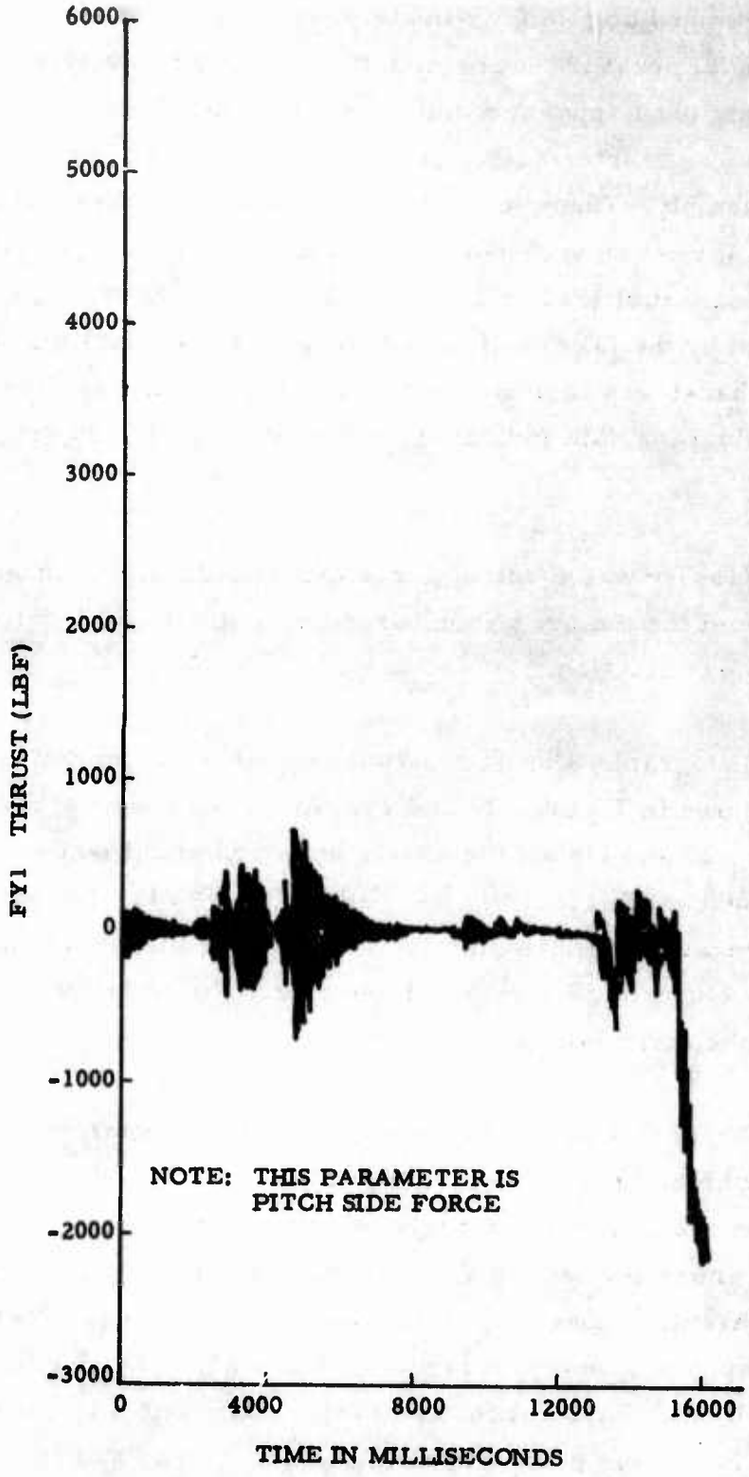

Figure 17. Pitch Force versus Time

The motor ignited with no pressure spike at approximately 600 psig. The pressure ramped up to approximately 800 psig at t=8 seconds. At that time, chamber pressure increased to 1200 psig and varied between 900 and 1400 psig until approximately 15.3 seconds. The case then burned through at the closure interface immediately opposite an upper-load-cell and flexure assembly. Chamber pressure then dropped to approximately 800 psig with a large variance between Pc_1 and Pc_2 readings. At t=18 seconds the axial thrust load cell apparently collapsed. The collapse was probably caused by the failure of the upper-load train resulting from burnthrough exhaust gas impingement. At t=19 seconds the closure was ejected. Oscillograph data indicated a maximum Pc of 1580 psig at 19 seconds.

After the closure was ejected, large masses of flaming propellant were thrown from the motor. No unburned propellant was located during postfire examination.

Postfire photographs showing melted regions of the motor closure and case are shown in Figures 18 and 19. An overall view of facility is shown in Figure 20 and the aft closure is shown where it landed (arrows) approximately 200 yards from the test pad in Figure 21. The materials sample arm recovered approximately 250 yards from the test pad and 70 yards from the closure, is shown in Figure 22. No useful data was obtained from the materials test.

The test nozzle was not damaged by its in-flight experience or the impact upon landing. The G-90 graphite throat performed quite well, experiencing an average surface regression rate of 3.25 mil/second. The castable-carbon sections of the entrance cap and exit cone eroded badly, and apparently experienced regression by chunking. Postfire nozzle photographs are shown in Figures 23 and 24. The chunking mode was evidenced by the sharp corners and irregular contours of the nozzle components. An erosion profile is shown in Figures 25 and 26.

TABLE III

SIGNIFICANT EVENT SEQUENCE

VISUAL DATA		
EVENT	TIME	SOURCE
Actuator In	2.22	1000 fps camera
Actuator Out	4.25	1000 fps camera
Smoke	8.56	1000 fps camera
First Flame	8.96	1000 fps camera
Pronounced Flame	9.66	1000 fps camera
Motor Goes Left	16.1	64 fps camera
Motor Goes Right	17.4	64 fps camera
Closure Ejection	18.32	200 fps camera
DIGITAL DATA		
EVENT	TIME	SOURCE
Actuator In	2.10	X_1 Reading
Actuator Out	7.0	X_1 Reading
Motor Goes Left	16.3	Y_1 Lost
Motor Goes Right	17.7	Z_A Lost, Roll Produced
Closure Ejected	19.3	Pc Lost

Figure 18. Aft Closure Damage

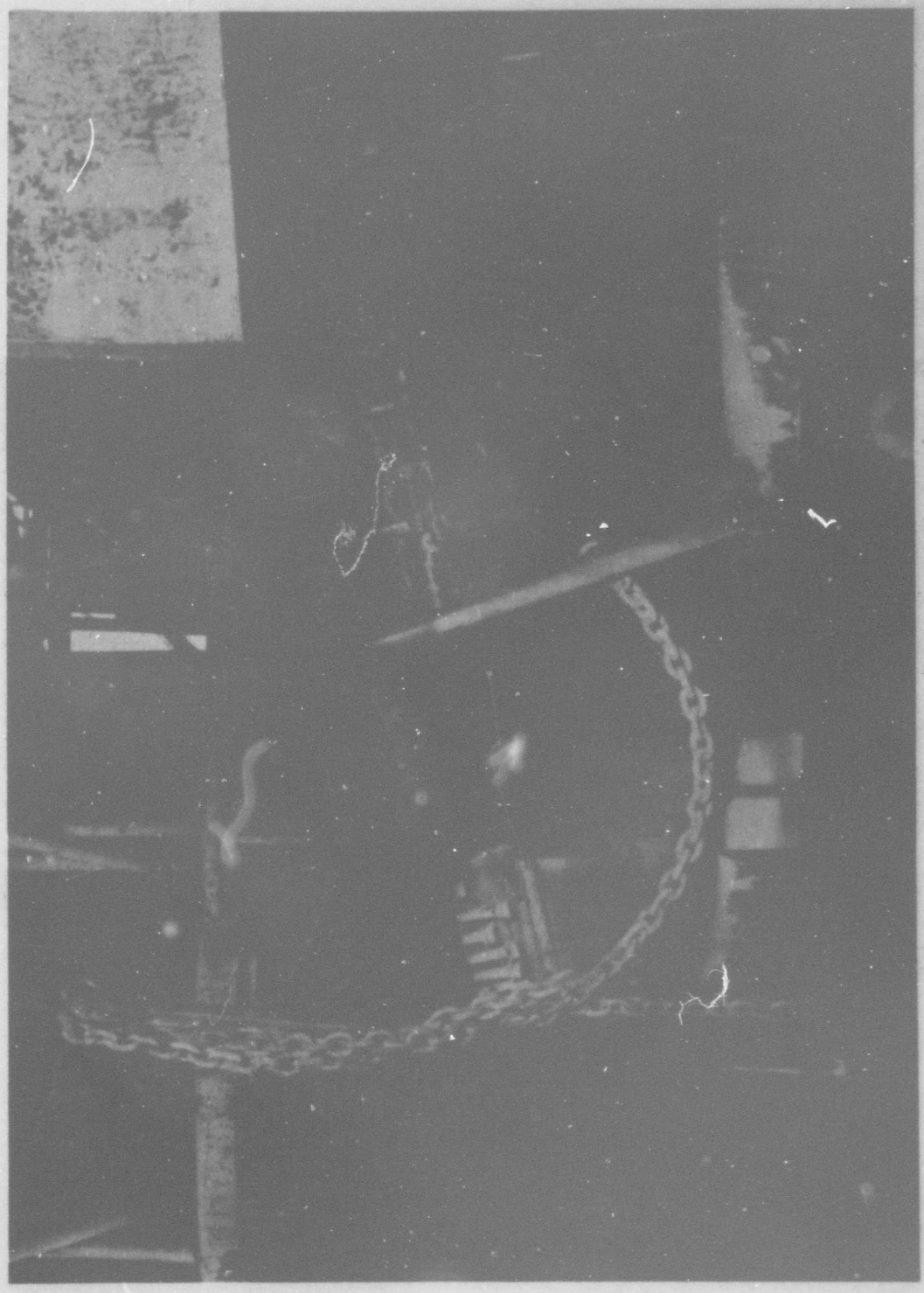

Figure 19. Motor Case Damage

Figure 20. Overall View of Facility Damage

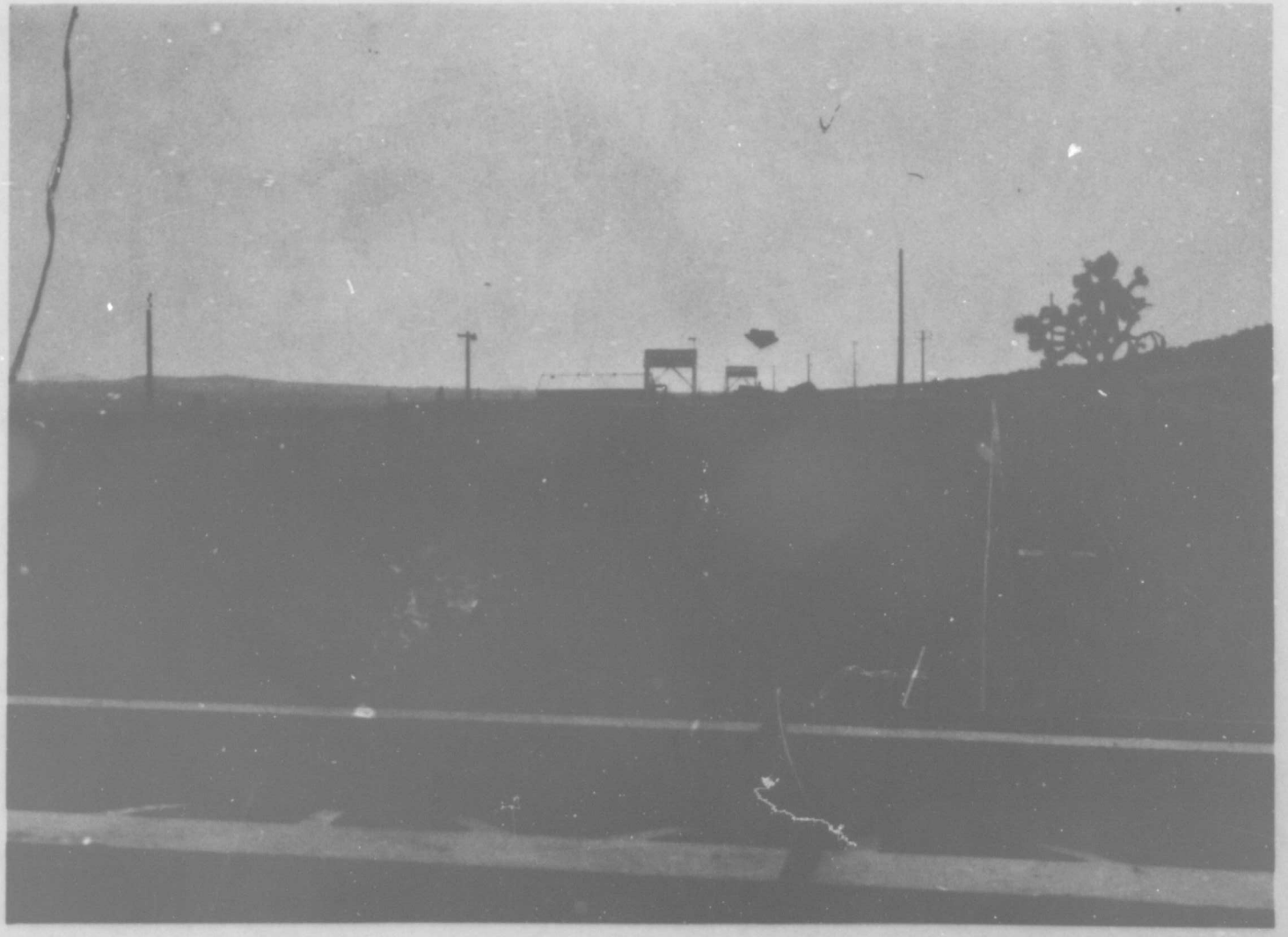

Figure 21. Aft Closure Location

Figure 22. Remains of Materials Test Fixture

Figure 23. Postfire Entrance Cone

Figure 23. Postfire Entrance Cone

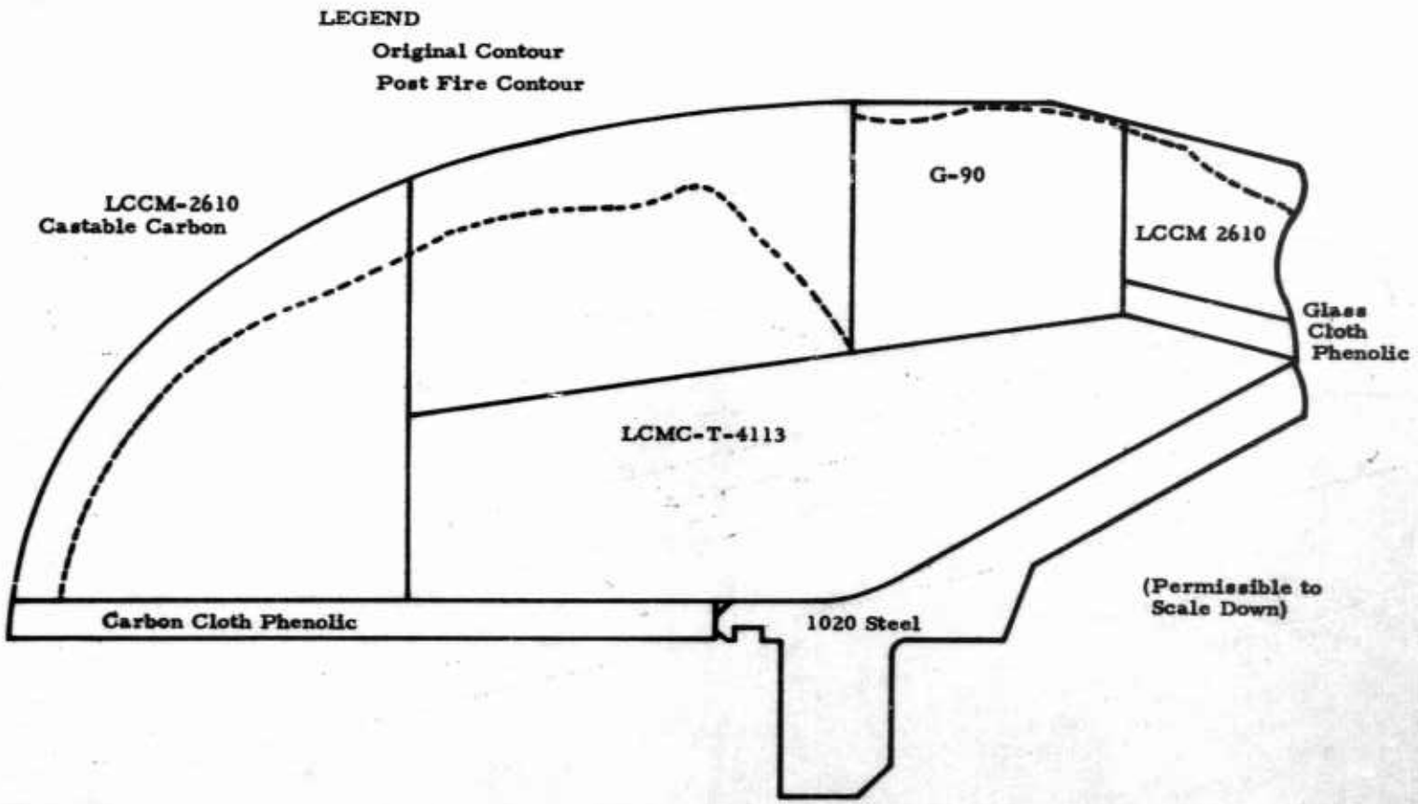

Figure 25. Erosion Profile

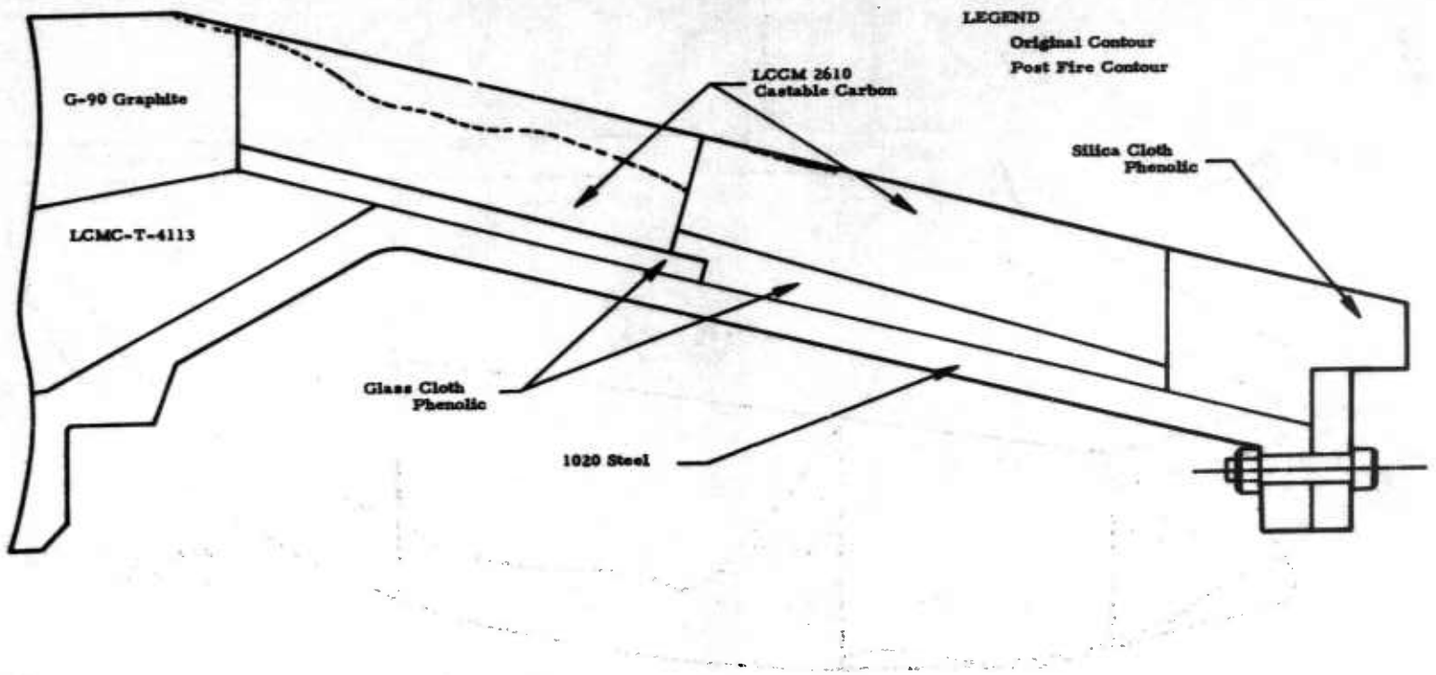

Figure 26. Erosion Profile

SECTION III

ACCIDENT INVESTIGATION

A four-phase accident investigation was initiated immediately after the motor failure. The first phase was to gather and examine all the test hardware that could be recovered. The second phase was to logically examine the motor performance in the light of successful 7-inch motor tests and other 36-inch motor tests. Personnel not associated with the program were consulted in order to provide an objective evaluation. The third phase was to formulate and execute a plan for active investigation of theories proposed in phase two. The fourth and last phase was to formulate conclusions and document all of the investigation activity.

A. PHASE I - EXAMINATION OF RECOVERED HARDWARE

A close inspection of all recovered hardware was performed. The burnthrough occurred exactly underneath one arm of the blast pad materials test fixtures (Figures 7 and 8) and was evidenced by the melted areas of both the closure and motor case (Figures 18 and 19). Another significant fact uncovered by the posttest examination was the failure of the two burst ports to function at their design rupture pressure. The only factor which could have affected their performance was a thin undercoating of rigid V-61 insulation. This had been applied because a burst disk burnthrough had been experienced on a previous test firing.

The following observations were made concerning the aft closure attachment to the motor case:

1. All but 9 of the 80 bolts holding the aft closure to the char motor failed by shearing the threads in the nuts. Physical evidence for this observation included damaged bolt threads, and material from the nuts remaining in the bolt threads.

2. The remaining 9 bolts appeared to have failed either by being cut by flame (during the burnthrough), by tensile fracture, or by a combination of both. No indication of shear failure of the nuts was found.

3. After the aft closure was located, four nuts were removed to allow disassembly of the bracket from the aft closure. A fifth bolt did not have a nut on it. The nut had not been in place when the closure impacted after ejection as is evidenced by Figures 28 and 29.

The thrust stand was severely damaged, and it was determined that all load cells and flexures would have to be replaced. Major structural components of the stand will be repaired and reused.

B. PHASE II - EXAMINATION OF CHAR MOTOR PERFORMANCE AND PROBABLE CONTRIBUTING FACTORS

Ten items were proposed as possible contribution factors. The first eight were directly concerned with the motor overpressure and the last two were primarily concerned with the premature case burnthrough resulting from the overpressure. The burnthrough was considered premature because the failure occurred at only 1.4 times the motor MEOP (Maximum Expected Operating Pressure).

Possible causes for this test motor overpressure are listed and briefly discussed.

1. Propellant burning surface instability during combustion was proposed as a prime cause of the char motor overpressure. The probability of large masses of propellant leaving the surface during combustion was established. No cure for this problem would be available in any low-viscosity uncured formulation.

2. Oxidizer particle segregation at the propellant/insulation interface was considered. Concentration of small ammonium perchlorate particles (7.9 micron diameter in this formulation) would result in a

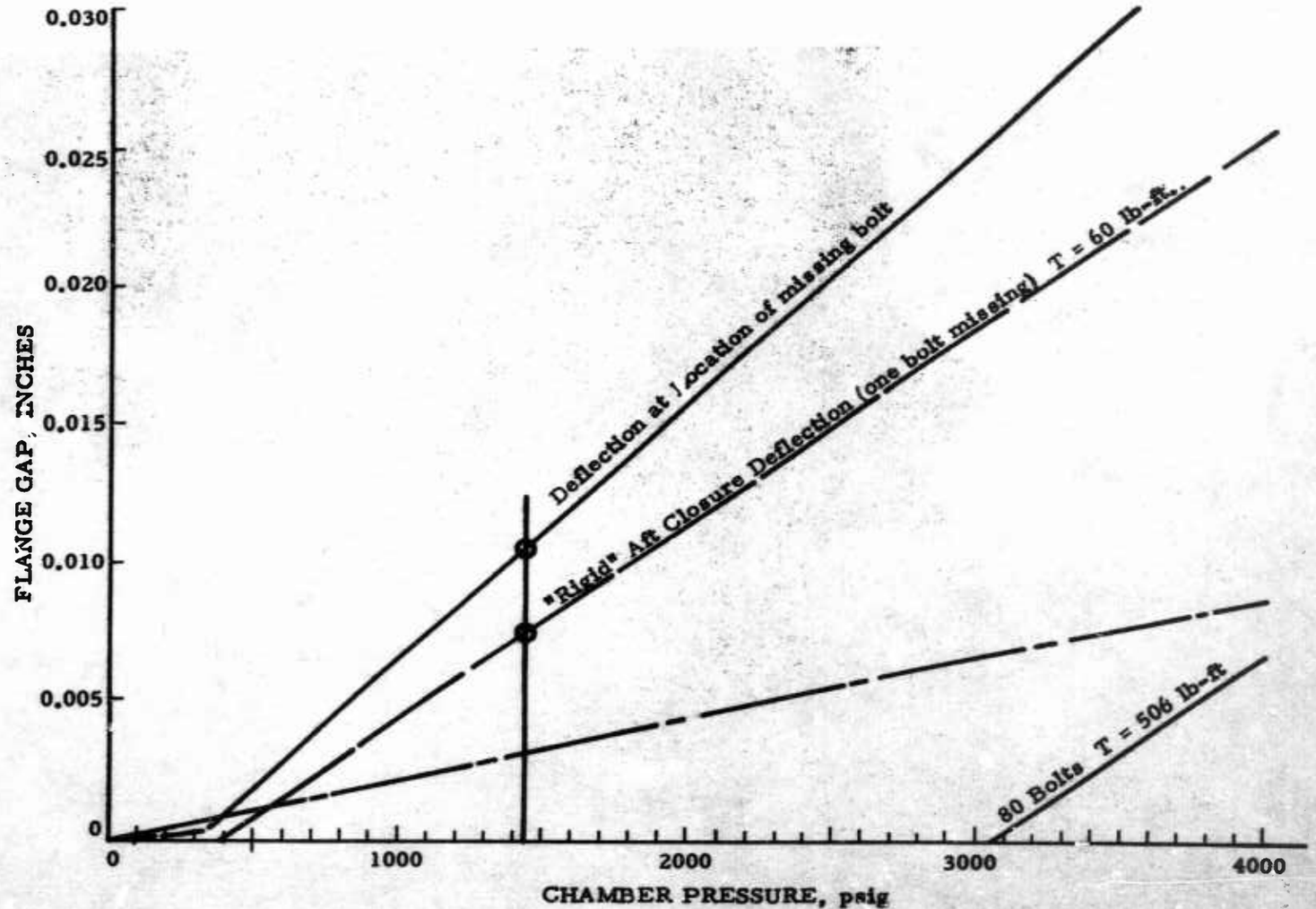

Figure 27. Gap Between Flanges with One Bolt Missing

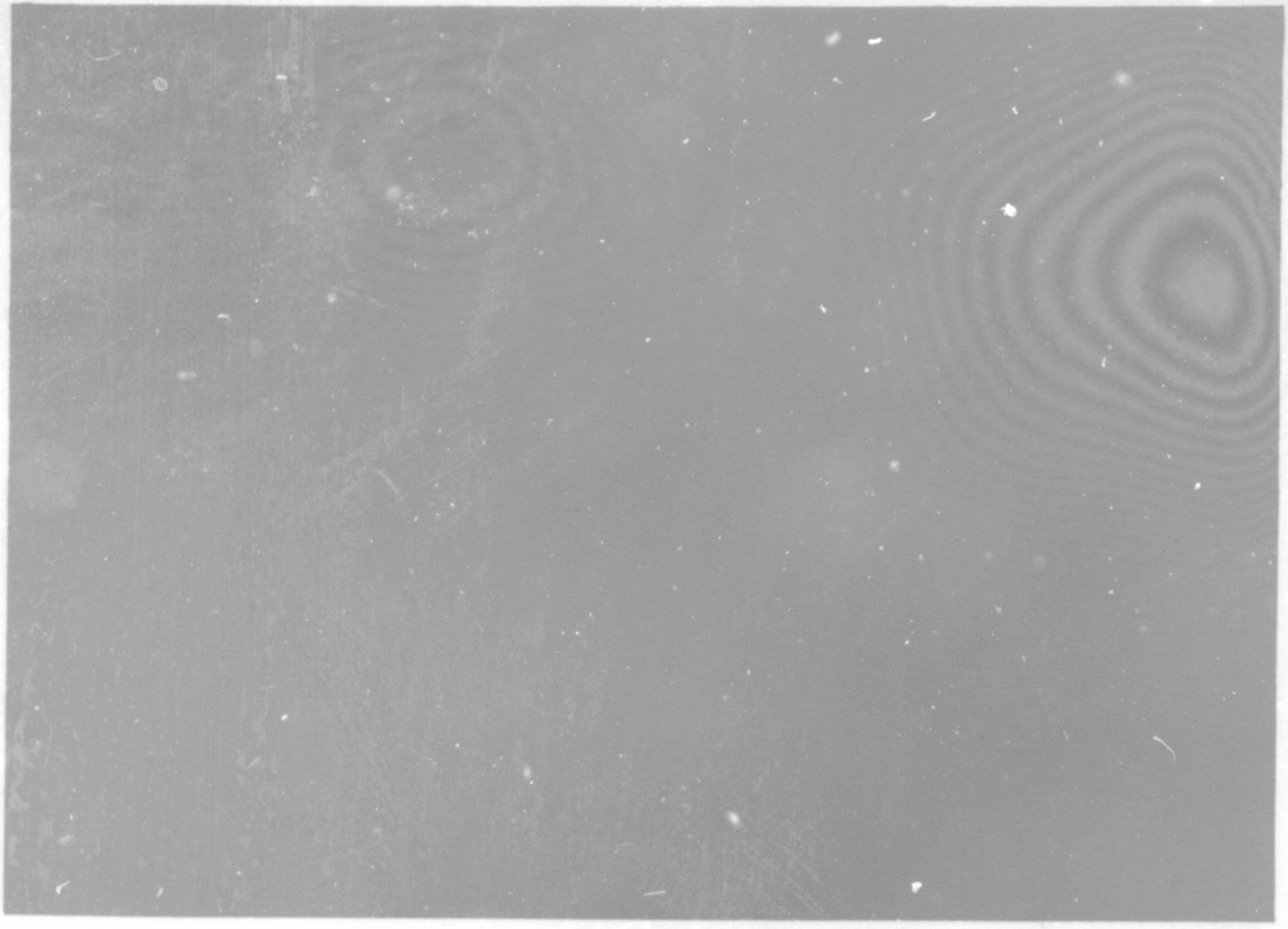

Figure 28. Questionable Bolt, Postfire

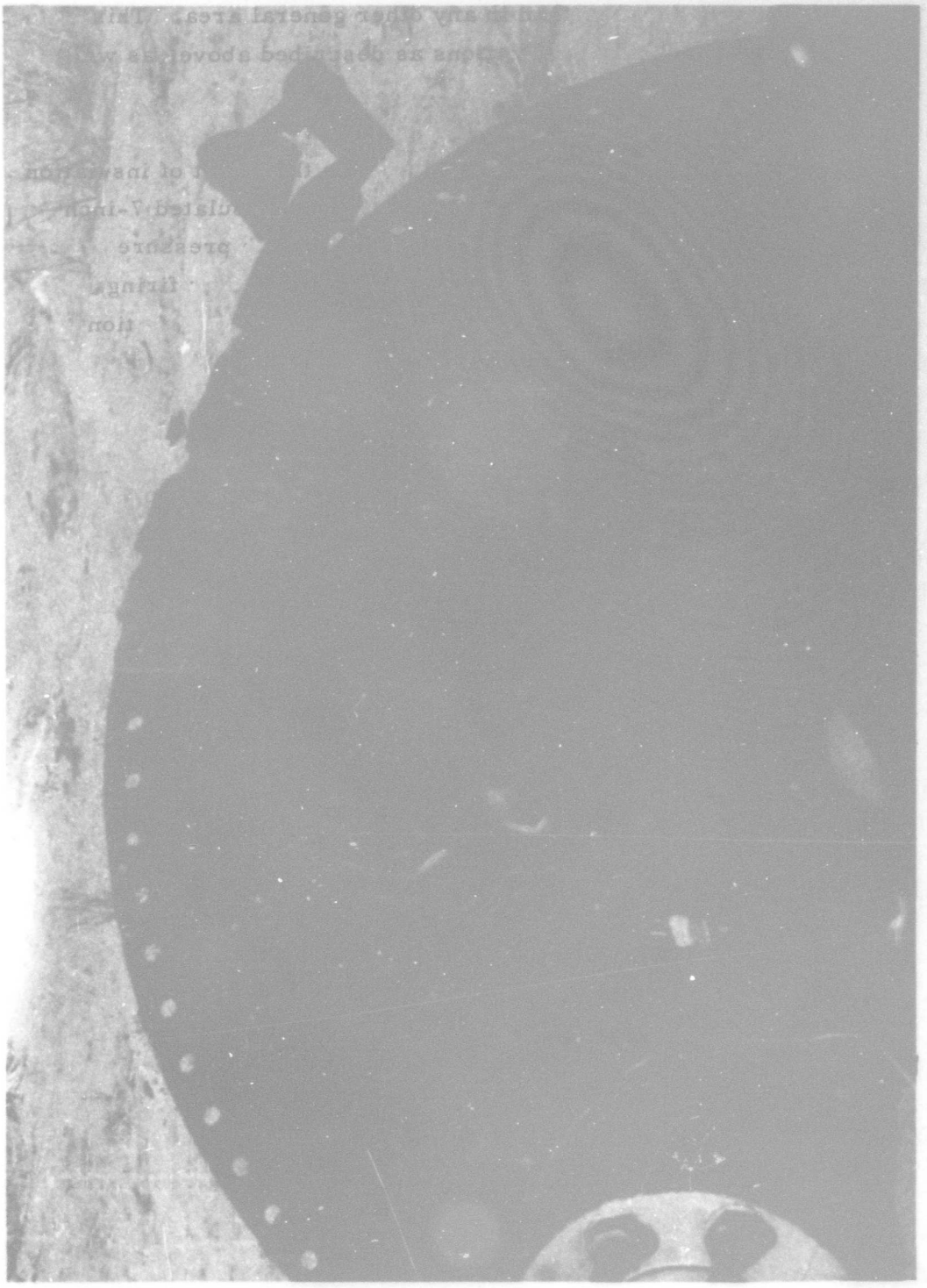

Figure 29. Questionable Bolt, Postfire

higher burn rate at the interface than in any other general area. This would induce propellant surface fluctuations as described above, as well as increase the burning surface area.

3. A logical extension of (2) was to consider the effect of insulation surface roughness upon the oxidizer segregation. V-61 insulated 7-inch motor firings were relatively successful exhibiting smooth pressure traces, while pressure traces from V-44 insulated char motor firings were chronically irregular. One difference between the two insulation materials was surface roughness. V-61 is relatively rough and may minimize any oxidizer segregation, while the smooth V-44 would be expected to contribute to the problem.

4. Differences in test preparations for the 7-inch motor firings and the 36-inch char motor firings were also considered. Differences were relatively minor, but one very significant factor emerged. All 7-inch firings were conducted with propellant taken from the upper layer of the storage drums. Char motor firings normally used a minimum of 3 drums. The propellant may not have been mixed well enough to provide a truly homogeneous mixture (the propellant was always hand-mixed to a uniform appearance with teflon paddles). The various levels of propellant could have significantly different burn rates because of variations in formulation.

5. The propellant formulation (LPC 634-A) included a burn-rate catalyst, n-butyl ferrocene, which accelerated the burn rate. Concentration gradients of this ingredient may also occur.

6. The possibility of a concave propellant burn surface was considered because of heat loss to the insulation near the propellent interface. Lower thermal flux could slow down the burn rate at the edge, cause a nonlevel surface, and result in a surface instability.

7. General observations included good motor performance in previous short-duration tests. This factor was not analyzed in detail because of its poor definition.

8. The last factor considered for the motor overpressure was associated with (4) above. Plasticizer had separated from the propellant after extended storage, and was mixed in by hand paddling. The possibility of plasticizer streaks being present was considered, and such a situation was verified during subsequent combustion bomb tests.

9. The first "nonballistic" factor considered was a missing nut in the region of the materials test fixture. This was based on the previously mentioned postfire hardware inspection.

10. The last hypothesis considered was the possibility of all bolts having improperly torqued nuts. This was examined in detail analytically and the results are discussed in the report.

C. PHASE III - INVESTIGATION ACTIVITY

The investigation activity was divided into two distinct tasks. A propellant performance investigation program using combustion bomb firings was conducted as a parallel effort with an extensive motor stress analysis task. The combustion bomb tests of the uncured propellant were conducted at 500 psig with high-speed motion picture coverage. The combustion bomb test objective was to determine whether or not uncured propellant experienced surface disturbances and/or burning at sidewall interfaces during combustion. The existence of both was verified.

The stress analysis was a three-phase effort, using: (1) a bolted joint - beam equivalent model; (2) a tension-compression deflection flange behavior model; and (3) a local deflection flange behavior model. The effects of a missing bolt were computed with the third model as well as the effects of bolt preload (torque) on flange separation. The analysis

results are contained in the following section, and the derivation of behavior models and calculations are in the Appendix.

D. PHASE IV - RESULTS OF INVESTIGATION PROGRAM

1. High-speed motion pictures indicate that the following sequence of events occurred:

a. A pressure leak in the vicinity of the bracket.

b. A subsequent, gradually developing burnthrough in this same area, centered at the flange interface.

c. Finally, a sudden ejection of the entire closure.

2. The combustion bomb firings were conducted by the COMETS (combustion) project at AFRPL, and will be documented in a future technical report under that project. The firings did show conclusively that the LPC 634-A propellant experienced repeated side-burining and combustion surface disturbances. The degree of side-burning and surface disturbances varied and were not predictable. Combustion bomb firings of high-viscosity, low-burn-rate uncured propellants were conducted as control firings because of the predictable performance of these propellants in earlier Char motor tests. The predictable, stable performance of these formulations in the combustion bombs contrasted with the results obtained with the LPC 634-A.

3. All bolts were under-torqued. This was confirmed by a simple calibration of the pneumatic wrench used to assemble the motor. Each nut tightened with the tool was torqued only to 65 ft. -lbs.

4. Slag deposits on the bolt and post test photographs indicate that a nut was missing, at least in the later stages of the burnthrough.

5. Failure of eight bolts in the general area of the missing nut was of a different type from that experienced by the remainder of the bolts, with the more probable modes being tensile fracture and flame cutting.

6. A bolt stress analysis indicated that, even with zero bolt preload, the gap between the closure and case flanges could open to no more than 0.008 inches, assuming no bolt failure. The probability of O-ring failure under these circumstances seemed low.

7. All of the above factors supported the following failure hypothesis:

a. Either the nut was left off of the questionable bolt, or it was removed by vibration or other forces early in the firing.

b. The load which would have been carried by this bolt was transferred to adjacent bolts, possibly resulting in tensile fracture of these bolts (although examination of all other recovered hardware that the nuts would have sheared first).

c. High flange deflections occured at the location of the ineffective bolt or bolts, permitting the O-ring seal to be unseated and/or extruded in the local area.

d. The subsequent pressure leak initiated the flow of hot gases.

e. Additional bolts failed as the flame damage weakened them.

f. This process continued until the remaining bolts could no longer sustain the load imposed upon them. They failed almost instantaneously and the closure was ejected.

g. The maximum gap opening at a given pressure was calculated in the Appendix by adding the deflection due to rigid body motion of the

closure and the local deflections of the flanges. The equations developed were:

rigid body deflection:

$$y_o = 17.563\ (p-p_o)\left(\frac{L}{AE}\right)$$

$$= \frac{17.563\ (p-p_o)\ (3.56)}{\frac{\pi}{4}(0.625)^2\ (29\times10^6)}$$

$$= 7.028 \times 10^{-6}\ (p-p_o)$$

p being greater than p_o, where p_o is the pressure at which flange separation begins.

flange deflection:

$$y_{max} = 2.161 \times 10^{-6}\ p$$

Computations utilizing these equations are graphically presented in Figure 27. Note that the pressure level at which burnthrough occurred (1440 psig) produced a calculated flange gap of 0.0104 inches. Since this was nearly half the initial compression in the O-ring, it seems plausible that a burnthrough would occur under the conditions assumed (one bolt missing bolts torqued to 60 ft-lbs). Note also that the deflection under the missing bolt is significantly higher than in other locations ("rigid" aft closure deflection). The most important point to be observed is that the combination of a missing bolt and low torque values resulted in a deflection at 1440 psig which is higher than the deflection which (with a correct installation) should have occurred at 4000 psig.

SECTION IV

CONCLUSIONS AND RECOMMENDATIONS

A. NOZZLE MATERIAL

Final conclusions and recommendations peculiar to nozzle material performance are somewhat clouded by the erratic motor performance. When reviewing the results of this test in the light of the previous Cast-Carbon Nozzle tests, some performance trends are indicated.

1. The low-cost material connot successfully survive the regions of highest severity (i. e., the throat) in a rocket nozzle. In all the previous failures, the inadequate components were at or near the nozzle throat.

2. The low-cost material can be successfully utilized in the entrance and exit extention areas.

3. Material reproducibility is still a problem. This is evidenced not only by variable performance from nozzle to nozzle, but also within particular nozzles. The entrance and throat portions of this test nozzle provide an excellent example. These two components were produced from the same formulation did not perform in a similar fashion. The bond line between these two sections was readily visible in both the postfire regression profiles and the photograph. Their dissimilar performance was attributed to different material properties since they were both exposed to a similar environment.

The following tems are recommended to bring the performance of castable carbonaceous materials to a level commensurate with standard ablatives:

1. Investigate the fabrication process to determine the cause for the previously demonstrated nonreproducibility.

2. Obtain thermal and mechanical property data at ambient and elevated temperatures to permit more thorough design and analysis.

B. MOTOR MALFUNCTION

1. The overpressure probably resulted from propellant side-burning at the insulation interface and from uneven combustion across the propellant surface. The side-burning could be due to the combination of fine AP particles and inefficient "wetting" at the insulation interface.

2. The burst disks did not rupture at their designed failure point because of the stiffening effect of the V-61 insulation undercoating. The conclusion is based on brief discussions with the disk supplier technical representatives. The actual confirmation of this possibility by destructive testing of undercoated units will still be attempted.

3. The closure burnthrough/ejection occurred because of the overpressure, and indirectly because of improperly torqued bolts and/or a bolt with no nut. The possibility of human error in the omission of a nut is considered unlikely, but circumstantial evidence supports this possibility. The bolts were undertorqued because of ill-defined motor assembly procedures. Procedures were not adequately documented, and frequent changes in project personnel contributed to the problem.

C. FUTURE PREVENTIVE ACTIONS

Final recommendations based on the extent of the investigation are presented below:

1. Terminate all testing with LPC 634-A propellant. This decision was based on the propellant's past performance in 36-inch char

motor tests and observation of combustion surface instabilities and side-burning during combustion bomb firings.

2. Document correct motor assembly procedures using torque values calculated by stress analysis in a Standard Operating Procedures Format. Insure that they are rigidly followed.

3. Do not allow installation of any fixture held on by the closure attachment bolts without adequate design analysis.

4. Plan and carry out closer project engineer supervision of test crews to preclude any occurrence similar to that indicated by the circumstantial evidence of the nut omission.

5. Hand mixing of separated propellant plasticizer should not be considered for any formulation. Even though problems with plasticizer effects have been observed only in 634-A, the possibility of similar effects in other formulations exits.

6. The overall suitability of uncured propellant as a flexible, low-cost test vehicle should not be judged too harshly because of poor char motor performance with the high-burn-rate LPC 634-A formulation. Many other very successful tests have been conducted. Apparently low-burn-rate, high-viscosity formulations are suitable for test applications; and high-burn-rate, low-viscosity formulations such as LPC 634-A are not. A total of 101 "production" char motor tests have been conducted to date. Acceptable motor performance was achieved with numerous low-burn-rate propellant firings, while five out of the last seven firings with high-burn-rate propellants have been decidedly unsuccessful. The solution is to select a nozzle throat diameter small enough to utilize a known, well-performing low-burn-rate propellant formulation.

APPENDIX

STRESS ANALYSIS CALCULATIONS

APPENDIX

STRESS ANALYSIS CALCULATIONS

A-1 BOLT/FLANGE BEHAVIOR - METHOD I

This method of analysis was taken from M. F. Spotts, Mechanical Design Analysis (pp 96 - 98). A typical one - bolt - space section of the bolted joint is treated as a beam (of length equal to the combined flange thickness) loaded by the bolt force and by the pressure load to be carried by the joint (see sketch).

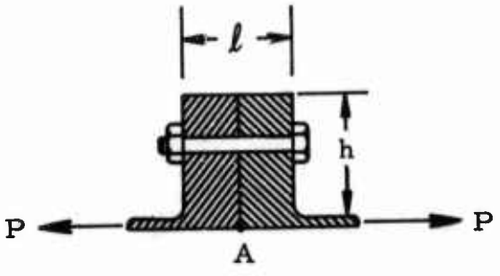

Bolted Joint

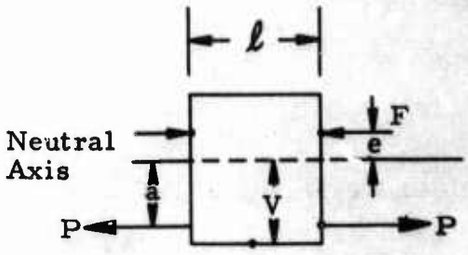

Equivalent Beam

The preload stress in the flange at point A is

$$s = -F_o \left(\frac{1}{A_2} + \frac{ev}{I}\right)$$ where A_2 is the net cross-sectional area of the flanges and F_o is the bolt preload. The stress at point A under load is

$$s' + s = P\left(\frac{1}{A_1+A_2} - \frac{av}{I}\right) + s$$

where A_2 is the bolt cross-sectional area.

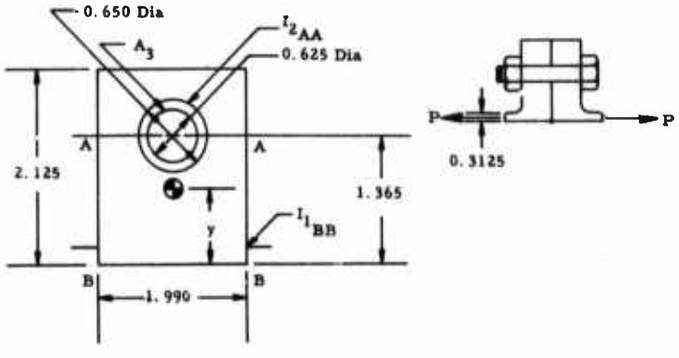

$$I_{2BB} = I_{2AA} + A_2 d^2 = 0.001272 + \frac{\pi}{4}\left[(.650)^2 - (.625)^2\right](1.365)^2$$

$$= 0.0479 \text{ in}^4$$

$$I_{1BB} = \frac{1}{3}bh^3 = \frac{1}{3}(1.990)(2.125)^3 = 6.365$$

$$I_{BB} = I_{1_{BB}} - I_{2_{BB}} = 6.317 \text{ in}^4$$

$$\bar{y} = \frac{A_1 d_1 - A_2 d_2}{A_1 - A_2} = \frac{2.125(1.990)(1.0625) - \frac{\pi}{4}\left[(.650)^2 - (.625)^2\right](1.365)}{(2.125)(1.990) - \frac{\pi}{4}\left[(.650)^2 - (.625)^2\right]}$$

or $\bar{y} = 1.0607$ in

$$I_{CC} = I_{BB} - A\bar{y}^2 = 1.587 \text{ in}^4$$

preload stress in flanges = $s = -F_o\left(\frac{1}{A_2} + \frac{ev}{I}\right)$ = contact pressure between flanges

where F_o = bolt preload,

A_2 = effective flange area

$= (2.125)(1.990) - \frac{\pi}{4}(.650)^2 = 3.897 \text{ in}^2$

e = distance from centroid to bolt ℄ (Positive upward)

v = distance (to fiber for which stress is to be determined) from centroid

I = moment of inertia of effective cross section

$$S = -F_o\left(\frac{1}{3.897} + \frac{(1.365-1.0607)(-1.0607)}{1.587}\right)$$

$$= -F_o(0.2566 - 0.19315) = -0.0532F_o$$

pressure load only:

stress in flange = $s = P\left(\frac{1}{A_2+A_3} - \frac{av}{I}\right)$

where P = pressure load on flange

A_2 = flange effective area
A_3 = bolt area

$$A_2 + A_3 = 2.125(1.990) - \frac{\pi}{4}\left[(.65)^2 - (.625)^2\right] = 4.204 \text{ in}^2$$

a = distance from neutral surface to P

= +0.7482 in (absolute value)

v = distance to fiber = $-\bar{y}$ = −1.0607 in

$$s' = P\left(\frac{1}{4.204} - \frac{(+0.7482)(-1.0607)}{1.695}\right)$$

$$= P\ (0.2378 + 0.4677) = 0.706\ P$$

Now $P = \dfrac{p\ \frac{\pi}{4} D^2}{\pi\ D_P}\ (1.990) = (1.990)\dfrac{p\ D^2}{4\ D_P}$ where D = I.D. of motor

D_P = diameter of neutral surface of motor wall

$$P = \frac{p(1.990)(42)^2}{4\ (42.625)} = 20.588\ p\ \frac{\text{lbs}}{\text{bolt}}$$

So $s' + s = (20.588p)(0.706) - 0.0532F_o$

<u>for separation to just begin at point A,</u>

$$s' + s = 0, \quad \text{or } F_{o\ \min} = \frac{(20.588)p\ (0.706)}{0.0532}$$

$$= 273\ p$$

The recommended preload for $\frac{5}{8}$ inch ASTM A 325 bolts, (tensile strength 125,000 psi) is 17,300 lb, equivalent to a torque of 180 lb-ft.

With this preload, separation will occur when

$$P = \frac{17,300}{273} = 63.4 \text{ psi}$$

Note that if the load P could be applied on the bolt centerline, a = 0 and

$$s' = \frac{P}{A_2 + A_3} = \frac{20.588p}{4.204} = 4.897p$$

$$s + s' = o = 4.897p - 0.0532F_o$$

$$F_{o\ min} = \frac{4.897p}{0.0532} = 92.05p$$

and, for a preload of 17,300 lb

$$p = \frac{17,300}{92.05} = \underline{187.9}\ \text{psi}$$

A-2 BOLT/FLANGE BEHAVIOR - METHOD II

The previous method ignores the stiffness of the shell at the point of attachment of the flange. In the present case, the resulting value of pressure required to separate flanges seems ridiculously low. Another approach which can be taken is to ignore the bending of the flanges and the shell, considering only the direct (tension-compression) deformations in the bolts and flanges. This method is taken from J. E. Shigley, Machine Design, pp 186-187.

From Shigley,

$$F = \frac{k_m F_t}{k_b + k_m} - F_1$$

where F = compressive force between flanges, F_t = separation load on flanges, F_i = bolt preload,

$$k_m = \frac{A_m E_m}{\ell_m}, \quad k_b = \frac{A_b E_b}{\ell_b}$$

Where m refers to the flange members, b refers to the bolt.

but $\ell_6 = \ell_m$;

Assume $E_m = E_b$

then
$$\frac{k_m}{k_b + k_m} = \frac{\frac{A_m E_b}{\ell_b}}{\frac{A_b E_b}{\ell_b} + \frac{A_m E_b}{\ell_b}} = \frac{A_m}{A_b + A_m}$$

From the motor geometry,

$$A_m = \frac{\frac{\pi}{4}\left(d_o^2 - d_i^2\right) - n\frac{\pi}{4} d_b^2}{n}$$

Where n = number of bolts d_o = flange o.d., d_1 = flange i.d., and d_b = diameter

$$= \frac{\pi}{4n}\left(d_o^2 - d_i^2\right) - \frac{\pi}{4} d_b^2$$

$$= \frac{\pi}{4}\left[\left(\frac{d_o^2 - d_i^2}{n}\right) - d_b^2\right]$$

And $A_m + A_b \cong \frac{\pi}{4}\left(\frac{d_o^2 - d_i^2}{n}\right)$

Substituting $n = 80$, $d_o = 46.250$ in., $d_i = 42,000$ in., and $d_b = 0.625$ in,

and $A_m = \frac{\pi}{4}\left[\frac{(46.25)^2 - (42)^2}{80} - (0.625)^2\right] = 3.375$ in

$$A_b + A_m = 3.682 \text{ in}$$

$$F_t = p\frac{\frac{\pi}{4} d_i^2}{n} = p\frac{\frac{\pi}{4}(42)^2}{80} = 17.318\,p \text{ lb/bolt}$$

So $$F = \frac{k_m F_t}{k_b + k_m} - F_i = \frac{3.375}{3.682}(17.318\,p) - F_i$$

or $$F = 15.874p - F_i$$

to keep the flanges from separating,

$$0 = 15.874p - F_i$$

$$F_i = 15.874\,p$$

and, if $F_i = 17,300$ (as recommended for ASTM/A325 bolts)

$$p = \frac{17,300}{15.874} = 1090 \text{ psi.}$$

However, the preload should be recalculated to utilize the higher strength of the bolts actually used (22,000 psi ultimate strength):

$$p = \frac{F_i}{15.874}$$

F_i recommended = .90 (proof load) (Shigley, p. 190)

$$\frac{\sigma u - \sigma p}{\sigma u} \cong 0.2 \quad \text{(based on Table 6-2, Shigley, p. 191)}$$

Where σu = ultimate tensile strength, σp = stress at proof load

$$\sigma p = -0.2\,\sigma u + \sigma u = 0.8\,\sigma u = 176,000 \text{ psi}$$

σ_i = preload stress = 0.9(176,000) = 158,000 psi

$$F_i = \sigma_i A_b = \sigma_i \frac{\pi}{4} (0.625)^2 = 48,600 \text{ lb}$$

$$T = 0.2(48,600)(0.625) = 6074 \text{ lb-in} = 506 \text{ lb-ft}$$

Calculations for different preloads are tabulated below and plotted on Figure 30.

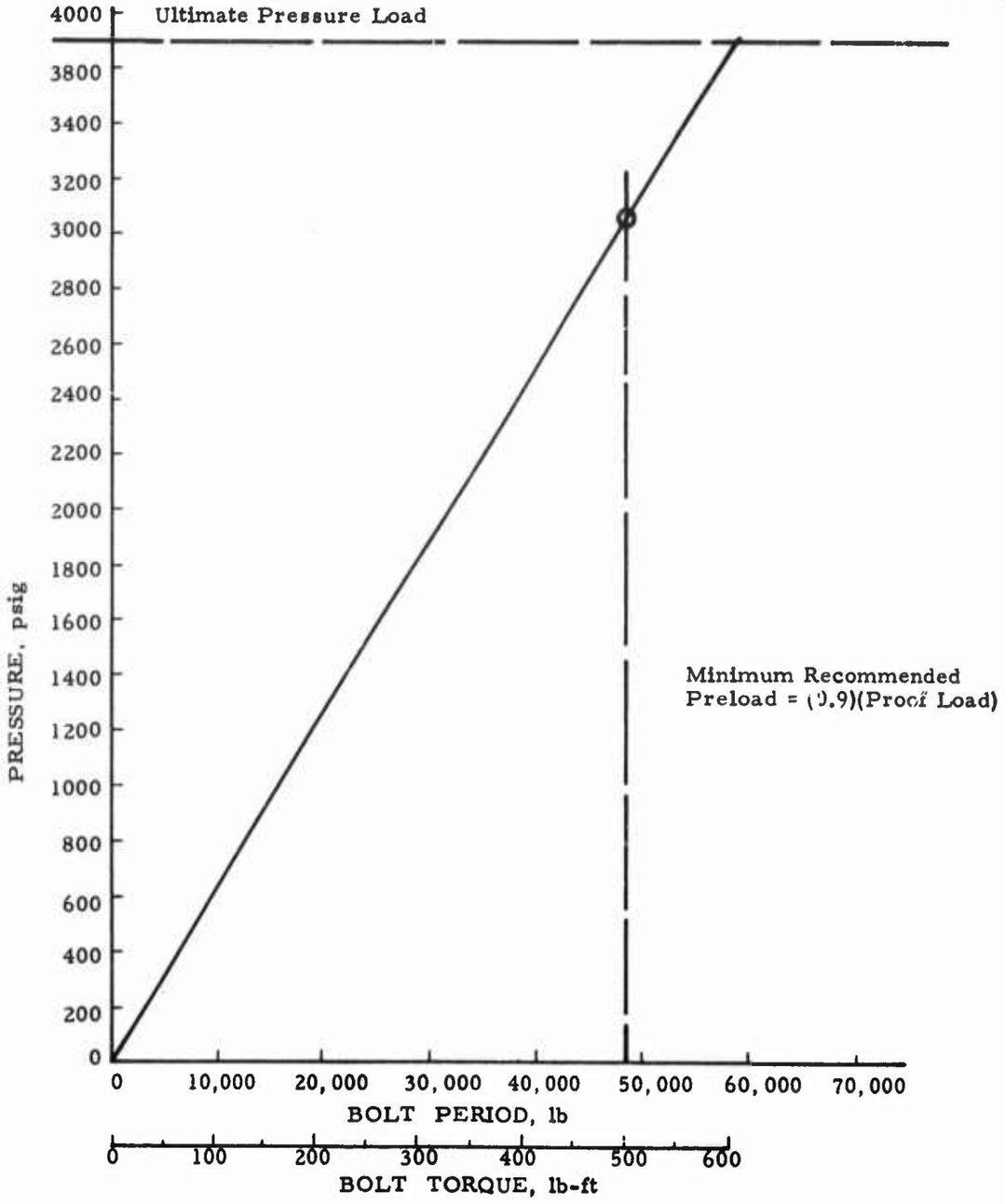

Figure 30. Pressure Required to Separate Flanges as a Function of Bolt Preload

F_i bolt preload, (lb)	P pressure for separation, (psi)	T equivalent torque, (lb-ft)
10,000	630	104
17,300	1090	180
20,000	1260	208
25,000	1575	260
30,000	1890	312
35,000	2205	364
40,000	2520	417
45,000	2835	469
48,000	3024	500
48,600	3062	506
50,000	3150	521
67,500	4252	703

To find the pressure corresponding to ultimate bolt load:

$$F_f = 17.318\ p \text{ lb/bolt}$$

$$\text{let } F_t = F_u = (220,000)\ \frac{\pi}{4}\ (0.625)^2 = 67,495 \text{ psi}$$

$$p_u = \frac{F_u}{17.318} = \frac{67,495}{17.318} = 3,897 \text{ psi}$$

Flange gap as a function of pressure (Rigid Flanges)

$$\text{Flange gap} = \sigma = \frac{F\,L}{AE} = 17.318\,(p - \rho_o)\left(\frac{L}{AE}\right)$$

Where L = bolt length
A = cross-sectional area
ρ_o = pressure at which flanges separate

$$= \frac{17.318(p - \rho_o)(L)}{\frac{\pi}{4}(0.625)^2(29\times10^6)} = 1.947\times10^{-6}\ (\rho - \rho_o)\ L$$

$$L_1 = 1.560 + 2.000 = 3.560 \text{ in.}$$

$$\sigma_{L_1} = 3.560\ (1.947\times10^{-6})(p - \rho_o) = 6.94\times10^{-6}(p - \rho_o) \text{ in.}$$

$$L_2 = L_1 + 0.500 = 4.060 \text{ in.}$$

$$\sigma_{L_2} = 4.060\ (1.947\text{x}10^{-6}) = 7.9\text{x}10^{-6}\ (p - p_o) \text{ in.}$$

The results are plotted in Figure 31.

Effect of Missing Bolts - Rigid Flanges

If the bolts are not equally stressed, the the flange gap will not be constant but will vary around the motor circumference. To account for this effect, the net cross section of the bolts will be considered as a "beam" under combined tensil and bending loads:

$$\sigma = \frac{M\,c}{I} + \frac{P}{\Sigma A}$$

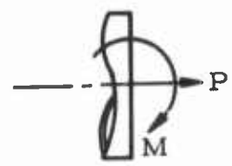

$$F_{max} = \text{max force per bolt} = \left(\frac{M\,c}{I} + \frac{P}{\Sigma A}\right) A_b = \frac{M_C}{I} A_b + P\,\frac{A_b}{n A_b}$$

$$= \frac{M\,c}{I} A_b + \frac{P}{n} = P\left(\frac{-\bar{y}c}{I} A_b + \frac{1}{n}\right)$$

$\bar{y}$, $I\bar{y}$, and c were calculated for various numbers of missing bolts:

Number of Missing Bolts

	none	1	3	5	7	9
$\bar{y}$, in	0	-0.283	-0.8695	-1.4818	-2.1182	-2.777
$I\bar{y}$, in^4	492,281	492,133	491,029	483,033	486,394	483,371
c, in	22.365	22.2961	22.0896	21.7471	21.2704	20.66257
n	80	79	77	75	73	71

but $P = 17.318p$, so $F_{max} = 17.381p\left(\frac{-\bar{y}\,c}{I} A_b + \frac{1}{n}\right)$

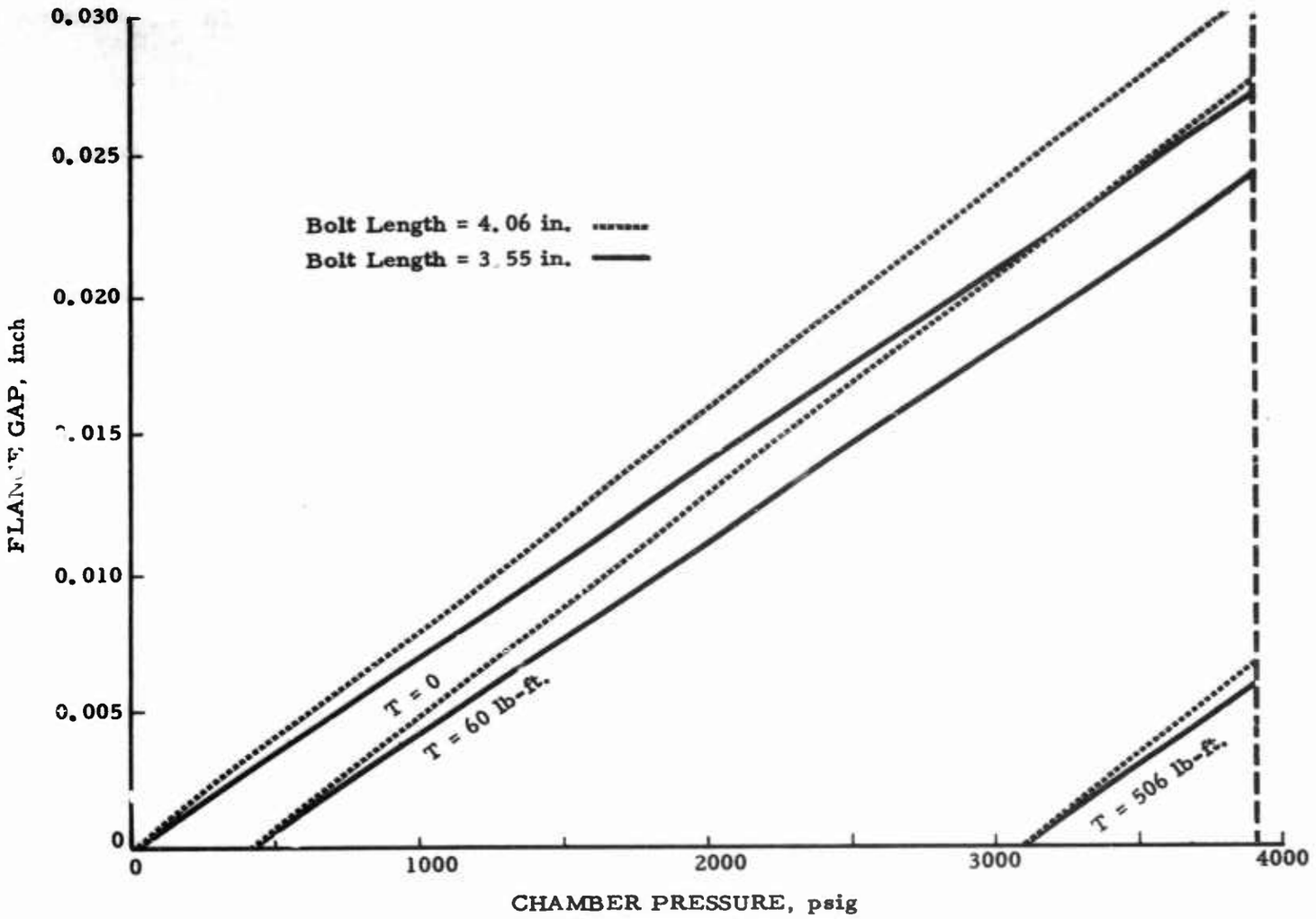

Figure 31. Effect of Bolt Preload on Flange Gap (Rigid Flanges, 80 Bolts)

No. of Bolts Missing	F_{max}	F_{ave}
0	17.320p	17.320p
1	17.544p	17.536p
3	18.008p	17.992p
5	18.504p	18.472p
7	19.016p	18.976p
9	19.56p	19.51p

The above results indicate that the effect of eccentricity is negligible when 1 to 9 bolts are missing from the bolt circle; i.e., the load is evenly distributed among the bolts. Therefore the flange gap may be considered to be the same at any point on the flange circumference if the flange remains rigid.

A-3 LOCAL DEFLECTION OF FLANGES

Under concentrated bolt loads, the closure and motor case flanges will deflect as shown in the sketch below:

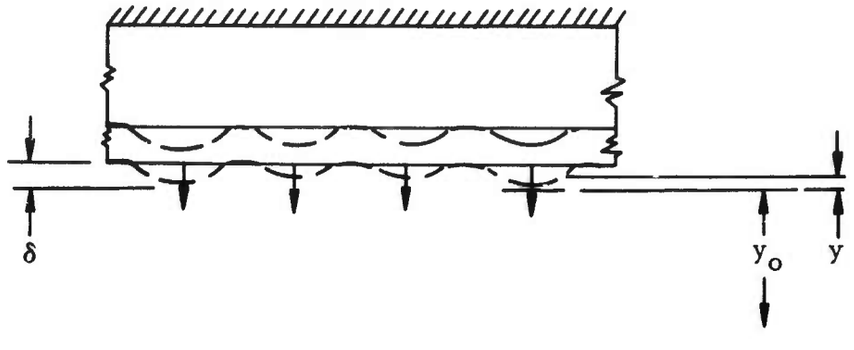

If y_o is the gap opening due to bolt deformation, then the total gap opening is $y_o + y_{\text{closure flange}} + y_{\text{case flange}}$.

The local flange deflection y is obtained by treating each flange as an infinite beam on an elastic foundation. The method is taken from Den Hartog, Advanced Strength of Materials, pp. 141 - 147.

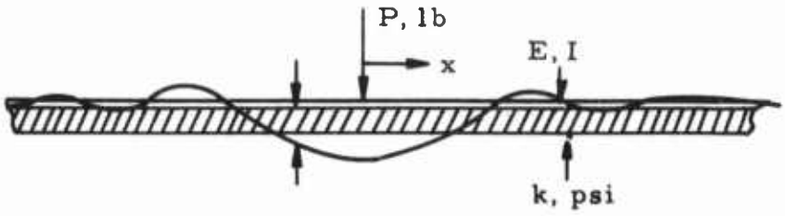

For a beam on an elastic foundation loaded with a concentrated load P, the deflection will have the form $\delta = \frac{P\beta}{2k} e^{-\beta x}(\cos \beta x + \sin \beta x)$

or $\delta = \frac{P\beta}{2k} F_1(\beta x)$

where $k = \frac{\text{load per unit length}}{\text{deflection}}$ for foundation

and $\beta = \sqrt[4]{\frac{k}{4EI}}$

$F_1(\beta x)$ is plotted (from Den Hartog, p. 146) in Figure 32.

Evaluation of k and β:

$$k = \frac{\text{load per inch}}{\text{deflection}} = \frac{q}{y}$$

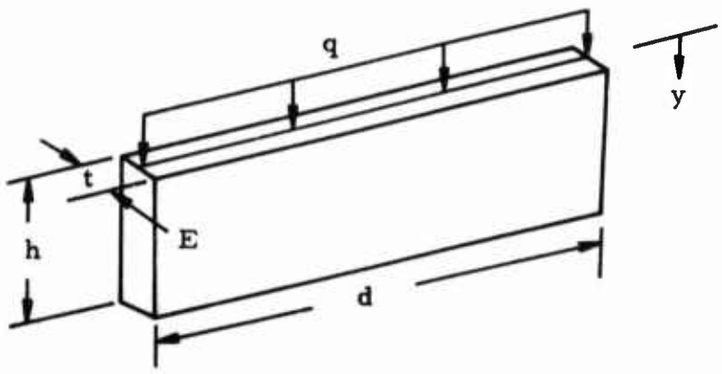

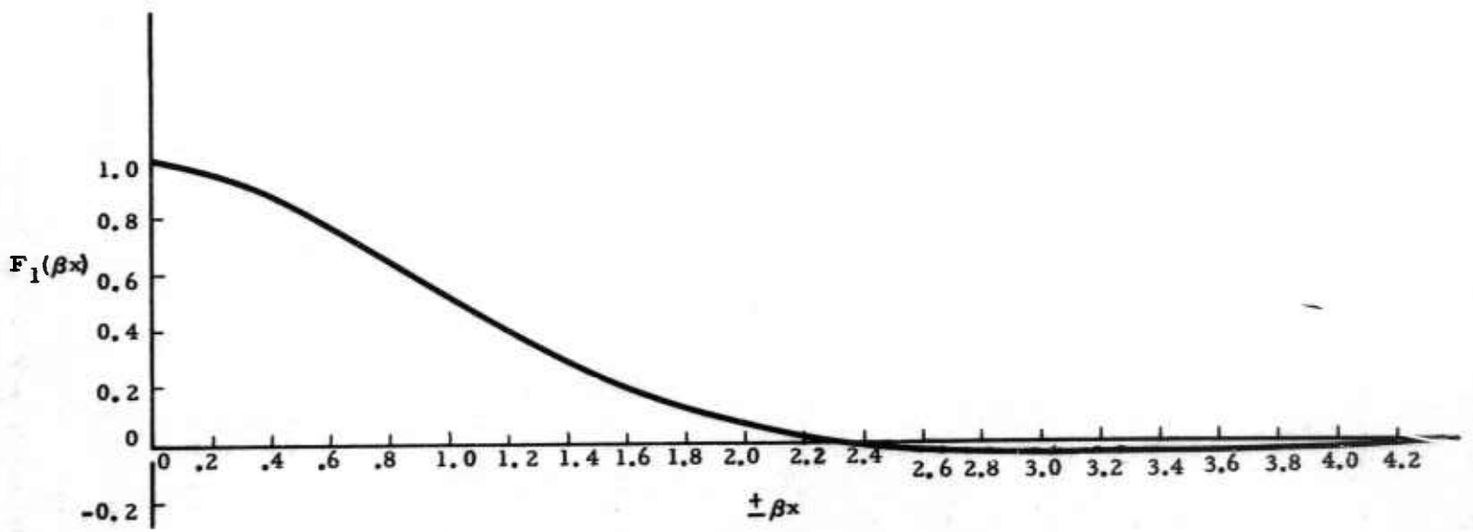

Figure 32. Deflection of Infinite Beam on Elastic Foundation

$$y = \frac{P\ell}{AE_1} = \frac{qdh}{t(d)(E_1)} = \frac{qh}{tE_1}$$

$$k = \frac{q}{y} = \frac{q}{qh/tE_1} = \frac{tE_1}{h}$$

assume $h \approx 10t$; then $k = \frac{E_1}{10} = \frac{E}{10}$

$$\sqrt[4]{\frac{k}{4EI}} = \sqrt[4]{\frac{E/10}{4EI}} = \sqrt[4]{\frac{1}{40I}}$$

For motor flange, $I = \frac{1}{12}(2.17)(1.560)^3 = 0.6865 \text{ in}^4$

For closure flange, $I = \frac{1}{12}(2.125)(2.000)^3 = 1.4167 \text{ in}^4$

For motor flange,

$$\beta = \sqrt[4]{\frac{1}{40(0.6865)}} = 0.4368$$

$$k = E/10 = 2.9 \times 10^6$$

For closure flange, $\beta = \sqrt[4]{\frac{1}{40(1.4167)}} = 0.3645$

$$k = E/10 = 2.9 \times 10^6$$

Deflection Due to Multiple Loads:

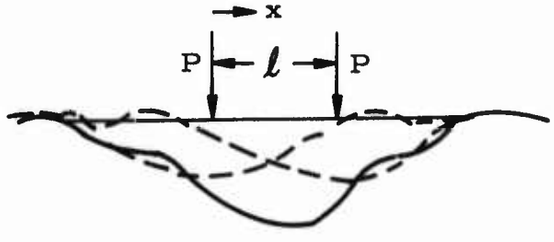

When two concentrated loads are present, acting a distance ℓ apart, the deflection can be obtained by combining the individual deflections for each load acting alone (see sketch above). Mathematically,

$$\delta = \frac{P\beta}{2k}\left[F_1(\beta x) + F_1(\beta x + \beta \ell)\right]$$

This procedure can obviously be extended to the case where a large number of loads are present. It becomes more convenient to replace x with ϕ, where

$$\phi = \frac{x}{\ell} = \text{Number of bolt spaces}$$

and $$F_1(\phi) = F_1\left(\frac{x}{\ell}\right) = F_1\left(\frac{\beta x}{\beta \ell}\right)$$

This function is plotted in Figure 33 for the motor case flange and in Figure 34 for the aft closure flange. Note that for the infinite beam, the deflection becomes a periodic function of wavelength $\phi = 1$. Since the influence of a single load is negligible at a distance of 6 or 7 bolt spaces, only ±6 (or 7) bolt spaces need be considered in determining the deflection curve.

We are interested in the gap opening

$$y_o + y_{closure} + y_{case} = y_o + (\delta_{max} - \delta)_{closure} + (\delta_{max} - \delta)_{case}$$

$$= y_o + y$$

These calculations are performed on the following pages. Figure 35 shows the deflection of the motor case flange alone (labeled "All Bolts Present").

Deflection with One Bolt Missing:

The deflection with one bolt missing is obtained by subtracting the deflection curve for a single bolt from the deflection curve for multiple bolts. That is, if $F(\phi)_{case} = \cdots F_1(\phi-6) + F_1(\phi-5) + \cdots + F_1(\phi) + \cdots + F_1(\phi+5) + F_1(\phi+6) + \cdots$ and $G_1(\phi) = F_1(\phi)$,

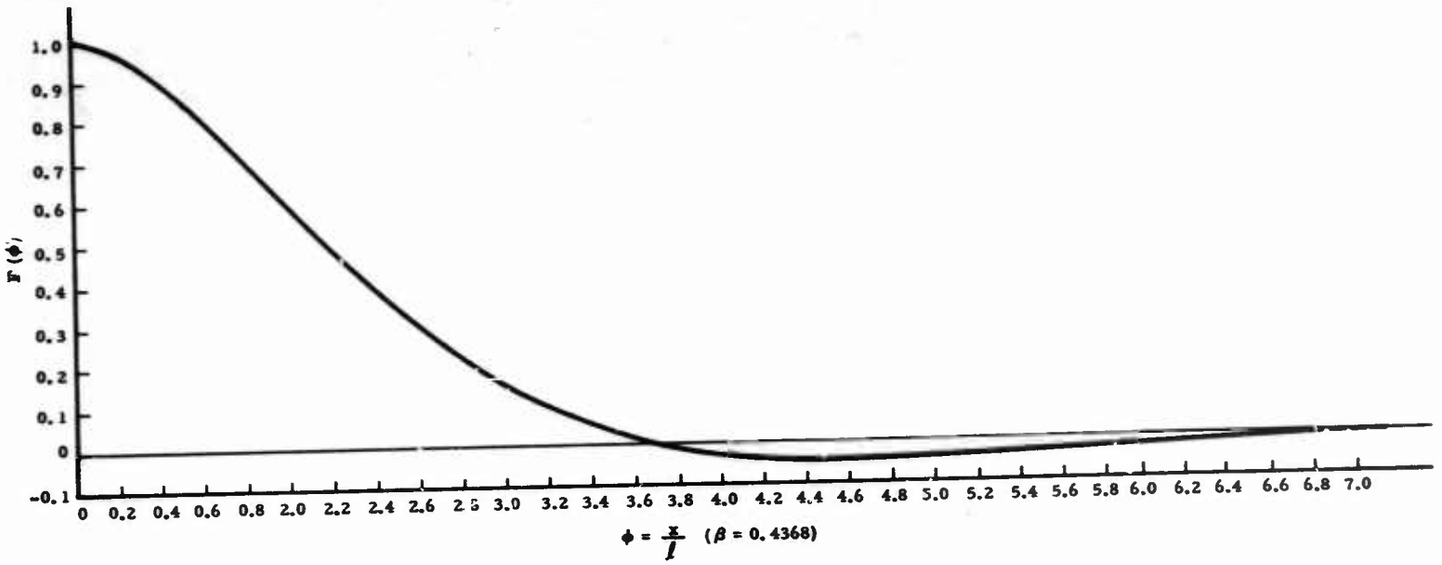

Figure 33. Deflection Function for Motor Case Flange

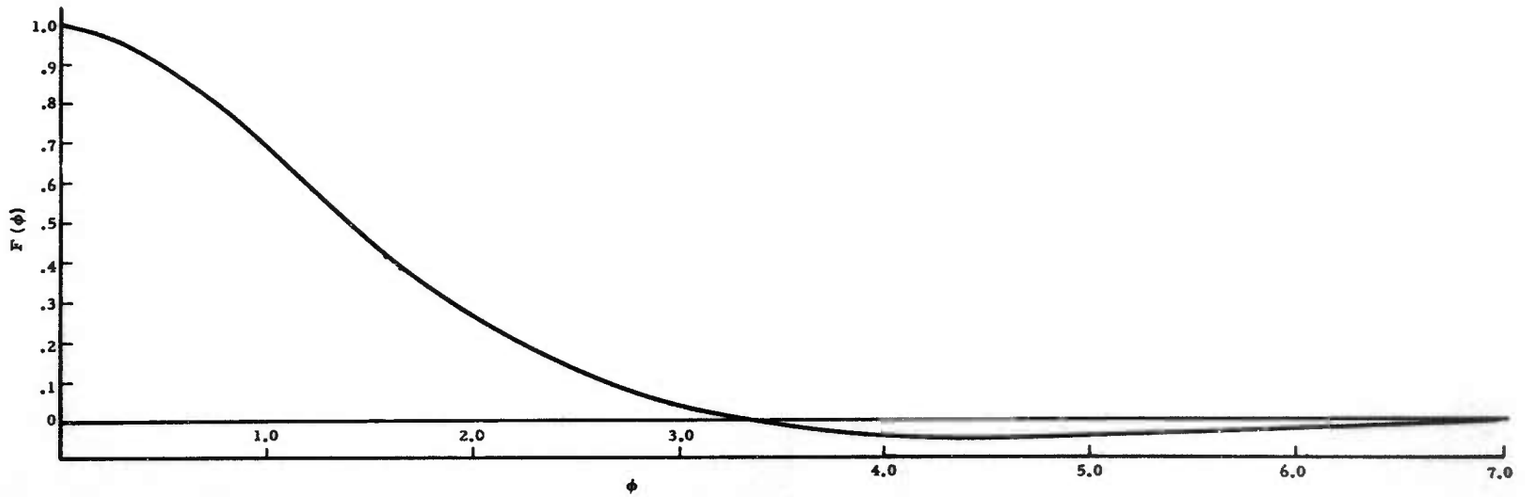

Figure 34. Deflection Function for Aft Closure Flange

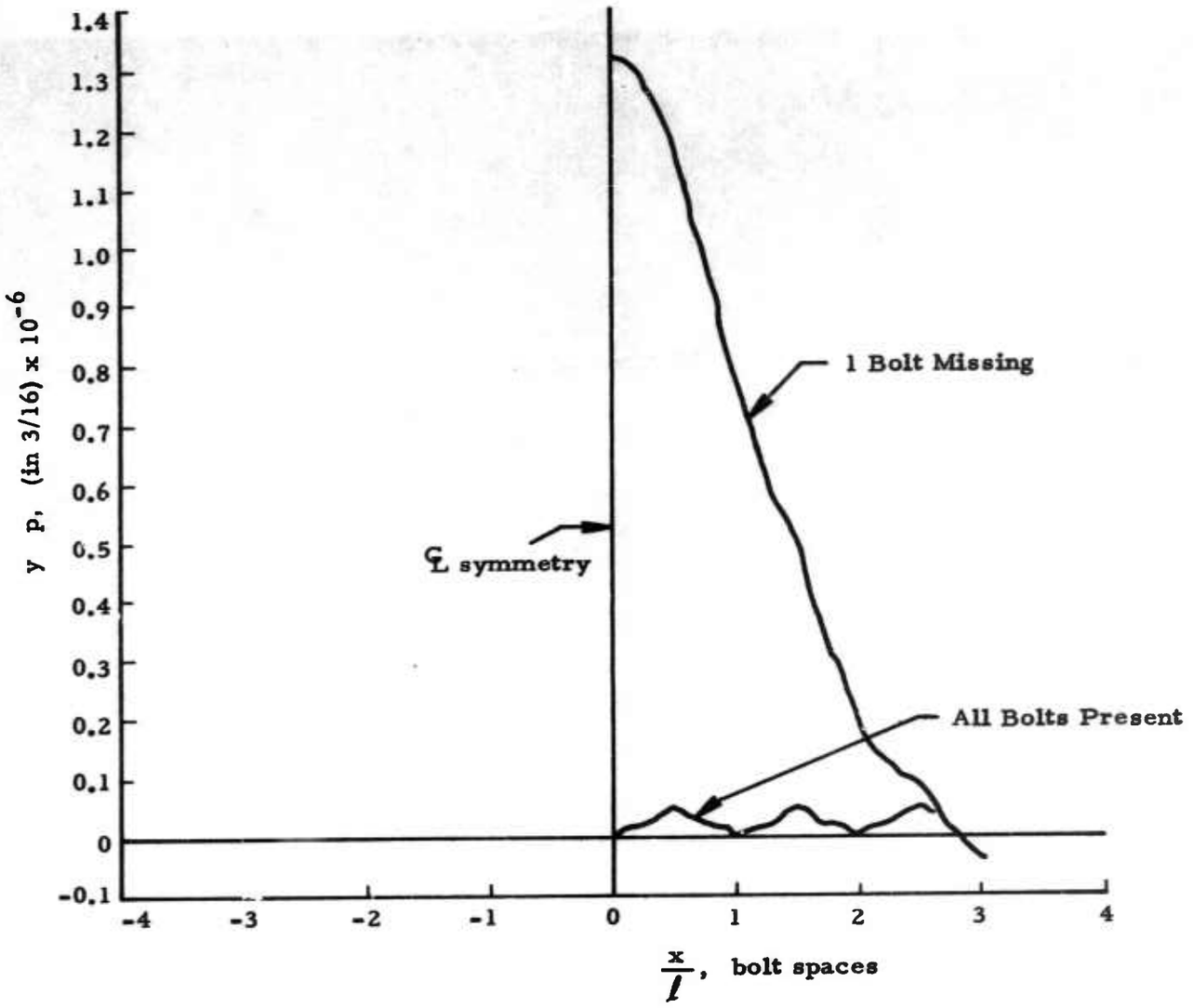

Figure 35. Local Deflection of Motor Case Flange

then $\delta_{case} = \frac{P\beta}{2k}\left[F(\phi) - G_1(\phi)\right]$, $y_{case} = \frac{P\beta}{2k}\left[F(\phi)_{max} - \left\{F(\phi) - G_1(\phi)\right\}\right]$

or $y_{case} = \frac{P\beta}{2k}\left[F(\phi)_{max} - F(\phi) + G_1(\phi)\right] = \frac{P\beta}{2k} F'(\phi)$

A similar process applies to the closure. These calculations are shown in Tables IV through IX. The deflection of the motor case flange alone, with one bolt missing, is shown in Figure 35.

TABLE IV. TABULATED CALCULATIONS – MOTOR CASE FLANGE

$F(n + \phi)$, n = number of bolts

ϕ	-6	-5	-4	-3	-2	-1	0	1	2	3	4	5
0	-.002	-.017	-.039	-.027	.146	.591	1.000	.591	.146	-.027	-.039	-.017
0.1	-.003	-.019	-.041	-.019	.177	.648	.993	.537	.118	-.032	-.038	-.016
0.2	-.006	-.020	-.041	-.010	.210	.702	.971	.482	.091	-.037	-.037	-.013
0.3	-.007	-.022	-.042	.000	.248	.758	.940	.430	.067	-.039	-.033	-.011
0.4	-.008	-.026	0.043	.013	.289	.806	.900	.380	.047	-.041	-.031	-.010
0.5	-.009	-.028	-.042	.029	.331	.854	.854	.331	.029	-.042	-.028	-.009
0.6	-.010	-.031	-.041	.047	.380	.900	.806	.289	.013	-.043	0.026	-.008
0.7	-.011	-.033	-.039	.067	.430	.940	.758	.248	.000	-.042	-.022	-.007
0.8	-.013	-.037	-.037	.091	.482	.971	.702	.210	-.010	-.041	-.020	-.006
0.9	-.016	-.038	-.032	.118	.537	.993	.648	.177	-.019	-.041	-.019	-.003
1.0	-.017	-.039	-.027	.146	.591	1.000	.591	.146	-.027	-.039	-.017	-.002

Note: Data taken directly from Figure 33.

TABLE V. TABULATED CALCULATIONS – MOTOR CASE FLANGE

ϕ	$F(\phi)$	$F(\phi)_{max}-F\phi$
0	2.306	0
.1	2.305	.001
.2	2.292	.014
.3	2.289	.017
.4	2.276	.030
.5	2.270	.036
.6	2.276	.030
.7	2.289	.017
.8	2.292	.014
.9	2.305	.001
1.0	2.306	0

$$F\phi = \cdots F_1(\phi-6) + F_1(\phi-5) + \cdots + F_1(\phi) + \cdots + F_1(\phi+5) + F_1(\phi+6) + \cdots$$

TABLE VI. TABULATED CALCULATIONS – MOTOR CASE FLANGE

ϕ	$G_1\phi$	$(F(\phi)_{max}-F\phi)$	$\frac{F'(\phi)z}{(F\phi_{max}-F\phi)+G_1\phi}$
0	1.000	0	1.000
±0.1	0.993	0.001	0.994
±0.2	0.971	0.014	0.985
±0.3	0.940	0.017	0.957
±0.4	0.900	0.030	0.930
±0.5	0.854	0.036	0.890
±0.6	0.806	0.030	0.836
±0.7	0.758	0.017	0.775
±0.8	0.702	0.014	0.716
±0.9	0.648	0.001	0.649
±1.0	0.591	0	0.591
±1.1	0.537	0.001	0.538
±1.2	0.482	0.014	0.496
±1.3	0.430	0.017	0.447
±1.4	0.380	0.030	0.410
±1.5	0.331	0.036	0.367
±1.6	0.289	0.030	0.319
±1.7	0.248	0.017	0.265
±1.8	0.210	0.014	0.224
±1.9	0.177	0.001	0.178
±2.0	0.146	0	0.146
±2.1	0.118	0.001	0.119
±2.2	0.091	0.014	0.105
±2.3	0.067	0.017	0.084
±2.4	0.047	0.030	0.077
±2.5	0.029	0.036	0.065
±2.6	0.013	0.030	0.043
±2.7	0	0.017	0.017
±2.8	-0.010	0.014	0.004
±2.9	-0.019	0.001	-0.018
±3.0	0.027	0	-0.027

Note: Deflection with all bolts present $= \left[F(\phi)_{max} - F(\phi)\right] \frac{P\beta}{2k}$

Deflection with one bolt missing $= \frac{P\beta}{2k} \left[F'(\phi)\right]$

TABLE VII. TABULATED CALCULATIONS – MOTOR CASE FLANGE

ϕ	$\frac{y(\phi)}{10^{-6}P}$
0	1.321
±0.1	1.313
±0.2	1.301
±0.3	1.264
±0.4	1.228
±0.5	1.176
±0.6	1.104
±0.7	1.024
±0.8	0.946
±0.9	0.857
±1.0	0.781
±1.1	0.711
±1.2	0.655
±1.3	0.590
±1.4	0.542
±1.5	0.485
±1.6	0.421
±1.7	0.350
±1.8	0.296
±1.9	0.235
±2.0	0.193
±2.1	0.157
±2.2	0.139
±2.3	0.111
±2.4	0.101
±2.5	0.086
±2.6	0.057
±2.7	0.022
±2.8	0.005
±2.9	-0.024
±3.0	-0.036

$$y(\phi) = \frac{P\beta}{2k} F'(\phi)$$

Note: These results are plotted in Figure 5.

Sample Calculation:

$$y = \frac{P\beta}{2k} F'; \quad k = 2.9 \times 10^6, \ \beta = 0.4368, \ P = 17.536p \text{ (bolt out, rigid flanges)}$$

$$y_{max} = \frac{17.536p\ (0.4368)}{2(2.9 \times 10)^6} \qquad F'_{max} = 1.321 \times 10^{-6} P$$

TABLE VIII. TABULATED CALCULATIONS – AFT CLOSURE FLANGE

$F(n+\phi)$

ϕ	-7	-6	-5	-4	-3	-2	-1	0.	1	2	3	4	5	6	$F(\phi)$
0	-.002	-.016	-.039	-.040	.031	.258	.686	1.000	.686	.258	.031	-.040	-.039	-.016	2.758
0.1	-.003	-.018	-.040	-.036	.043	.294	.732	.995	.635	.226	.018	-.042	-.034	-.013	2.757
0.2	-.004	-.019	-.042	-.032	.060	.333	.777	.980	.590	.200	.009	-.044	-.031	-.012	2.765
0.3	-.006	-.020	-.044	-.028	.078	.372	.819	.958	.540	.172	-.002	-.046	-.030	-.010	2.753
0.4	-.007	-.022	-.046	-.022	.099	.414	.859	.930	.496	.146	-.009	-.047	-.028	-.009	2.754
0.5	-.008	-.026	-.047	-.017	.121	.455	.896	.896	.455	.121	-.017	-.047	-.026	-.008	2.748
0.6	-.009	-.028	-.047	-.009	.146	.496	.930	.859	.414	.099	-.022	-.046	-.022	-.007	2.754
0.7	-.010	-.030	-.046	-.002	.172	.540	.958	.819	.372	.078	-.028	-.044	-.020	-.006	2.753
0.8	-.012	-.031	-.044	.009	.200	.590	.980	.777	.333	.060	-.032	-.042	-.019	-.004	2.765
0.9	-.013	-.034	-.042	.018	.226	.635	.995	.732	.294	.043	-.036	-.040	-.018	-.003	2.757
1.0	-.016	-.039	-.040	.031	.258	.686	1.00	.686	.258	.031	-.040	-.039	-.016	-.002	2.758

TABLE IX. TABULATED CALCULATIONS – AFT CLOSURE FLANGE

(Max $F(\phi)$ = 2.765) $\qquad$ $F(\phi)_{max}-F(\phi)+G_1(\phi) = F'(\phi)$

	$F(\phi)_{max}-F$		ϕ=0	1.	2.	3.
0	.007	.0	1.007	.693	.265	.038
0.1	.008	.1	1.003	.643	.234	.026
0.2	.000	.2	.980	.590	.200	.009
0.3	.012	.3	.970	.552	.184	.010
0.4	.011	.4	.941	.507	.157	.002
0.5	.017	.5	.913	.472	.138	.000
0.6	.011	.6	.870	.425	.110	-.011
0.7	.012	.7	.831	.384	.090	-.016
0.8	.000	.8	.777	.333	.060	-.032
0.9	.008	.9	.740	.302	.051	-.028
1.0	.007					

A-4 GAP DEFLECTION

The individual results computed for the case and closure flanges are combined in Tables X and XI on the following two pages. The total gap deflection for the flanges ($y_{case} + y_{closure}$) is plotted in Figure 36 for all bolts present and for one bolt missing.

TABLE X. TOTAL GAP DEFLECTIONS, ALL BOLTS PRESENT

ϕ	F_{case}	$\frac{y_{case}}{10^{-6}P}$	$F'_{closure}$	$\frac{y_{closure}}{10^{-6}P}$	$\frac{y_{case} + y_{closure}}{10^{-6}P}$
0.0	0	0	0.007	0.008	0.008
0.1	0.001	0.001	0.008	0.009	0.010
0.2	0.014	0.019	0.000	0	0.019
0.3	0.017	0.022	0.012	0.013	0.035
0.4	0.030	0.040	0.011	0.012	0.052
0.5	0.036	0.048	0.017	0.019	0.067
0.6	0.030	0.040	0.011	0.012	0.052
0.7	0.017	0.022	0.012	0.013	0.035
0.8	0.014	0.019	0.000	0	0.019
0.9	0.001	0.001	0.008	0.009	0.010
1.0	0	0	0.007	0.008	0.008

Notes:

1. $$y_{case} = \left(\frac{P\beta}{2k}\right)_{case} F'_{case} = \frac{17.536\rho\ (0.4368)}{2(2.9\times10^{-6})} = 1.321 \times 10^{-6}\rho\ F'_{case}$$

2. $$y_{closure} = \left(\frac{P\beta}{2k}\right)_{closure} F'_{closure} = \frac{17.536\rho\ (0.3645)}{2(2.9\times10^{-6})} = 1.102\times10^{-6}\rho\ F'_{closure}$$

3. $$(y_{case} + y_{closure})_{\phi} = (y_{case} + y_{closure})_{n+\phi},\ n = 1,\ 2,\ 3,\ \cdots$$

TABLE XI. TOTAL GAP DEFLECTION, ONE BOLT MISSING

ϕ	F_{case}	$\frac{y_{case}}{10^{-6}P}$	$F_{closure}$	$\frac{y_{motor}}{10^{-6}P}$	$\frac{y_{case} + y_{closure}}{10^{-6}P}$
0	1.000	1.321	1.007	1.110	2.431
±0.5	0.854	1.176	0.913	1.007	2.183
±1	0.591	0.781	0.693	0.764	1.545
±1.5	0.331	0.485	0.472	0.521	1.006
±2.0	0.146	0.193	0.265	0.282	0.475
±2.5	0.029	0.086	0.138	0.152	0.238
±3.0	-0.027	-0.036	0.038	0.040	0.004
±3.5	-0.042	-0.055	-0.000	-0.000	-0.055
±4.0	-0.039	-0.052	-0.043	-0.047	-0.099

Notes:

1. $$y_{case} = \left(\frac{P\beta}{2k}\right)_{case} F'_{case} = \frac{17.536\rho(0.4368)}{2(2.9\times10^{-6})} = 1.321\times10^{-6}\,\rho F'_{case}$$

2. $$y_{closure} = \left(\frac{P\beta}{2k}\right)_{closure} F'_{closure} = \frac{17.536\rho(0.3645)}{2(2.9\times10^{-6})}$$

$$= 1.102\times10^{-6}\,\rho F'_{closure}$$

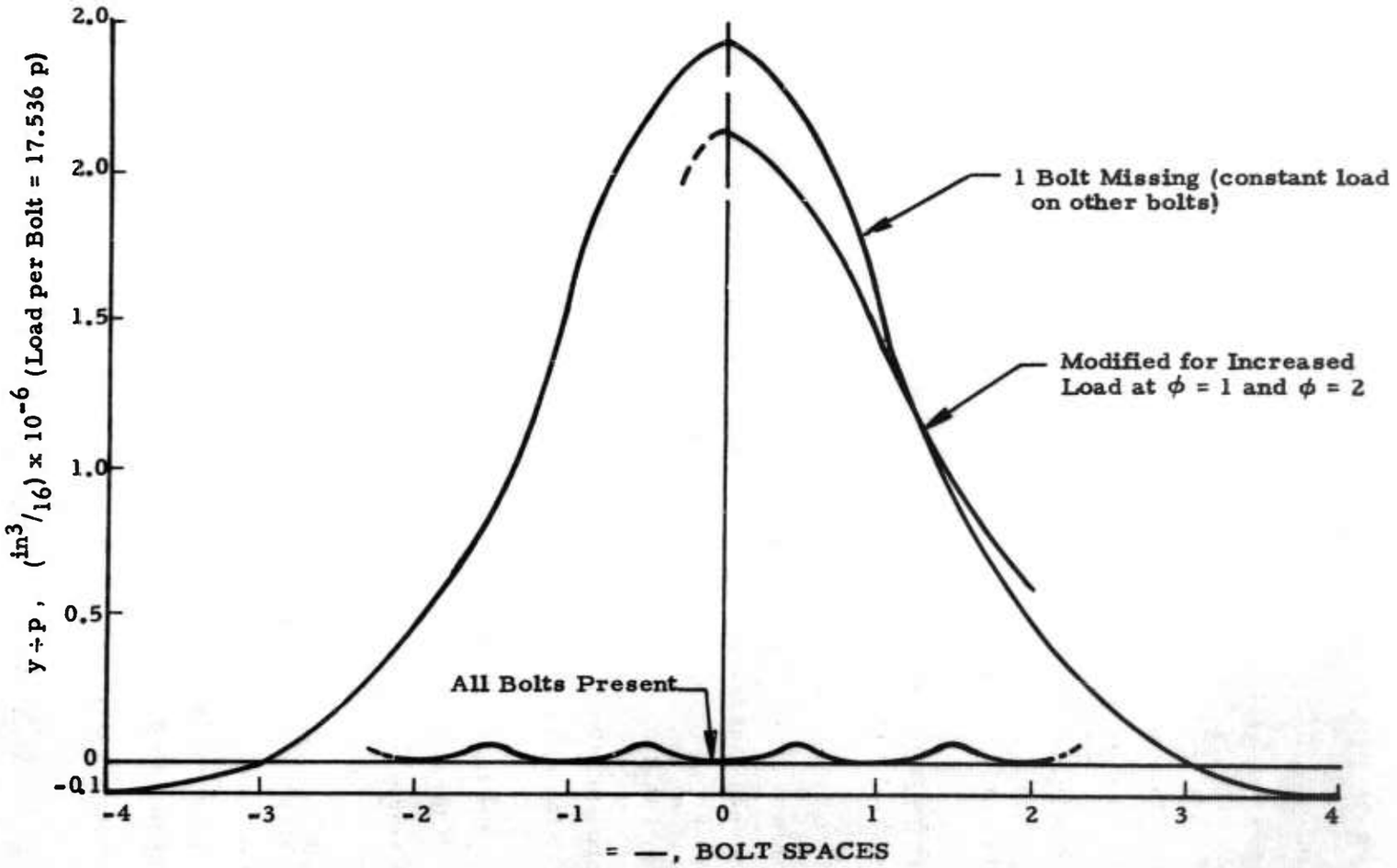

Figure 36. Combined Local Deflections of Motor Case and Closure Flanges

A-5 FORCES ON BOLTS ADJACENT TO MISSING BOLT

The deflection curve derived above (Figure 36) assumed that all bolts carry the same load. This assumption is in error for two reasons:

1. The nine bolts centered around the missing bolt are 1/2 inch longer than all the other bolts in the assembly. If all bolts had zero original preload and the closure experienced a rigid body displacement δ, then the forces in the longer bolts would be $P_2 = \frac{\delta AE}{\ell^2}$; those in the shorter bolts would be $P_1 = \frac{\delta AE}{\ell_2}$; therefore $\frac{P_2}{P_1} = \frac{\ell_1}{\ell_2} = \frac{3.56}{4.06} = 0.877$, or the longer bolts would exert about 88% of the force exerted by the shorter bolts.

2. The computed deflection curve indicates that a significant local deflection orrucs at the bolt locations near the missing bolt. The local deflection is such that the bolt will be "stretched" an additional amount over that which was computed for rigid flanges, which would result in a higher force at that point.

A better approximation of the deflection of the flanges can be achieved by correcting for the above discrepancies.

Consider the bolts at positions $\phi = 1$, $\phi = -1$. By symmetry, the load on both of these bolts is the same (P_1). As shown in Figure 36 and Table XI, a single force of -17.536P produces a maximum deflection of $+2.431p \times 10^{-6}$. A force of $\Delta P = p$ would then produce a maximum deflection of $(2.431_{p \times 10^{-6}})(\frac{1}{-17.536}) = -0.1384p \times 10^{-6} = -0.1384 \times 10^{-6} \Delta P$.

Following this logic, deflection influence coefficients may be obtained for pairs of bolts at positions 1 and 2, paying due attention to the symmetry of the problem:

change in deflection at $\phi = \pm 1$ due to ΔP_1:

$$\Delta y_{1,P_1} = k_{f_1} \Delta P_1; \quad k_{f_1} = \frac{-(2.431 + (.475)}{17.536p} \times 10^{-6} p = -0.1657 \times 10^{-6}$$

change in deflection at $\phi = \pm 2$ due to Δy_1:

$$\Delta y_{2,\,y_1} = k_{1-2}\,\Delta y_1; \quad k_{1-2} = \frac{(1.545 + .004)}{2.431} \times 10^{-6} = 0.637 \times 10^{-6}$$

change in deflection at $\phi = \pm 2$ due to ΔP_2:

$$\Delta y_{2,\,P_2} = k_{f_2}\,\Delta P_2; \quad k_{f_2} = \frac{-(2.431 - .099)}{17.536p}\,10^{-6}p = -0.1330 \times 10^{-6}$$

change in deflection at $\phi \pm 1$ due to Δy_2:

$$\Delta y_{1,\,y_2} = k_{2-1}\,\Delta y_2; \quad k_{2-1} = k_{1-2} = 0.637 \times 10^{-6}$$

The force in each bolt is $P_i = 17.536\,\frac{(3.56)}{4.06}\,p + k_b y_i$, or

$$P_i = 15.376p + k_b y_i, \text{ where } k_b = \frac{AE}{\ell} = \frac{\frac{\pi}{4}\,(.625)^2\,(29 \times 10^6)}{4.06};$$

$$k_b = 2.194 \times 10^6$$

An iterative procedure was used to determing P_1, y_1, P_2, and y_2 to satisfy the above equations. This was carried out by successively modifying the variables as follows:

$$P_1' = 15.375 + k_b y_1 \qquad (1)$$

$$y_1' = y_1 + k_{f_1}\,(P_1' - P_1) \qquad (2)$$

$$y_2' = (y_1' - y_1)\,k_{1-2} + y_2 \qquad (3)$$

$$P_2' = 15.376p + k_b y_2' \qquad (4)$$

$$y_1' = (y_2' - y_2)\,k_{1-2} + y_1 \qquad (5)$$

The initial values of y_1 and y_2 were taken from Figure 36. The final results of the iterative calculations were:

$$P_1 = 18.498p$$

$$y_1 = 1.424 \times 10^{-6}p$$

$$P_2 = 16.656p$$

$$y_2 = 0.584 \times 10^{-6}p$$

From Table XI, it can be shown that

$$\frac{y_{\phi=0}}{p \times 10^{-6}} = 2.431 + (1.424-1.545)(2)(1.545) + (0.584 - 0.475)(2)(0.475)$$

$$= 2.431 - 0.374 + 0.104 = 2.161$$

and $$y_{max} = y_{\phi = 0} = 2.161 \times 10^{-6}p$$

Further refinement of the deflection curve was not undertaken. The modified deflection curve is shown in Figure 36.

REFERENCES

1. Cardall, S. H., and Laramee, R. C.; "Castable Carbonaceous Insulation Development", Quarterly Technical Report No. 3, AFRPL-TR-67-51, AD 378868; Confindentail Report.

2. Ellison, J. R., and Ojala, S. J.; "Flexible Exit Cone Development Program - Materials Evaluation Test Results"; AFRPL-TR-69-25, February 1969; Unclassified Report.

Unclassified

Security Classification

DOCUMENT CONTROL DATA - R & D

(Security classification of title, body of abstract and indexing annotation must be entered when the overall report is classified)

1. ORIGINATING ACTIVITY (Corporate author) Air Force Rocket Propulsion Laboratory Edwards, California 93523	2a. REPORT SECURITY CLASSIFICATION Unclassified 2b. GROUP N/A

3. REPORT TITLE

Test Firing of a Castable Carbon Rocket Nozzle

4. DESCRIPTIVE NOTES (Type of report and inclusive dates)

Test Report - 30 October 1968

5. AUTHOR(S) (First name, middle initial, last name)

John R. Ellison, Lt, USAF; Robert J. Schoner; Durwood I. Thrasher

6. REPORT DATE February 1969	7a. TOTAL NO. OF PAGES	7b. NO. OF REFS 2
8a. CONTRACT OR GRANT NO. b. PROJECT NO. 3059 c. d.	9a. ORIGINATOR'S REPORT NUMBER(S) AFRPL-TR-69-39 9b. OTHER REPORT NO(S) (Any other numbers that may be assigned this report)	

10. DISTRIBUTION STATEMENT

This document is subject to special export controls and each transmittal to foreign governments or foreign nationals may be made only with prior approval of AFRPL (RPOR-STINFO), Edwards, California 93523.

11. SUPPLEMENTARY NOTES	12. SPONSORING MILITARY ACTIVITY Air Force Rocket Propulsion Laboratory

13. ABSTRACT

The test firing of a castable-carbon material nozzle was conducted 30 October 1968 on the AFRPL 36-inch-diameter char motor, utilizing the Gilmore six-component thrust stand. Samples of blast pad covering material were also tested by insertion into the exhaust plume. The motor overpressured and performed erratically until approximately 19 seconds after ignition when the aft closure was ejected. Prior to the ejection, a burnthrough was observed at the aft closure - motor chamber interface. The incident resulted in severe damage to the motor and thrust stand, with minor damage to the test pad and adjacent facilities. Planned duration and chamber pressure had been 56 seconds and 750 psig, respectively. The severe environment experienced by the nozzle allowed only limited acquisition of performance data. An accident investigation was initiated and the preliminary findings indicated that problems with the performance of uncured LPC 634-A propellant, characterized by massive side burning and possible burn-surface perturbations, caused the overpressurization. Improperly torqued closure attachment bolts allowed the burnthrough at the closure - motor interface. A description of stress analysis calculations performed for the bolted flange joint is provided.

DD FORM 1 NOV 68 1473

Unclassified

Security Classification

14. KEY WORDS	LINK A		LINK B		LINK C	
	ROLE	WT	ROLE	WT	ROLE	WT
Castable carbon						
Char motor						
Uncured propellant						
Motor case failure analysis						